



Investigation of conformation  
exchange of dimethylated arginine as a  
recognition motif

Untersuchung der Konformations-  
änderung dimethylierten Arginins als  
Erkennungsmotiv



**Bachelor's Thesis**

zur Erlangung des akademischen Grades eines

*Bachelor of Science*

der Fakultät für Chemie der  
Technischen Universität München

vorgelegt von  
Raphael Peltzer  
aus Köln

angefertigt am  
Lehrstuhl  
für biomolekulare NMR-Spektroskopie  
(Prof. Dr. Michael Sattler)  
unter der Anleitung von  
PD Dr. Gerd Gemmecker

Garching, Mai 2013

## Zusammenfassung

Symmetrisch und antisymmetrisch methyliertes Arginin(sDMA/aDMA) wird von Tudor Domänen gebunden, wodurch die Funktionalität der Tudor Domäne beeinflusst wird. Kristallstrukturen zeigen, dass sDMA nur in bestimmten Konformationen gebunden wird, welche sich durch Rotation um die  $C_\zeta - N_\eta$  Bindungen unterscheiden.

Im Verlauf dieser Arbeit wurden die Rotationen um die  $C_\zeta - N_\eta$  Bindungen und die  $C_\zeta - N_\epsilon$  Bindung untersucht, jedoch konnte in den aufgenommenen NMR-Spektren keine Rotationsbarriere für die  $C_\zeta - N_\eta$  Bindungen festgestellt werden. Da Spektren bis hinunter zu 200 K aufgenommen wurden ist davon auszugehen, dass die Rotationsbarriere der  $C_\zeta - N_\eta$  Rotation sehr niedrig ist. Die Aktivierungsenergie der  $C_\zeta - N_\epsilon$  Bindung wurde zu circa  $12 \text{ kcal mol}^{-1}$  bestimmt, abhängig vom Lösemittel und vom eingesetzten Gegenion. Die Aktivierungsenergie der  $C_\zeta - N_\epsilon$  Bindung für in Methanol- $d_3$  gelöstes aDMA mit HCl als Gegenion wurde also zu  $8.9 \pm 0.9 \text{ kcal mol}^{-1}$  bestimmt. Aus den errechneten Aktivierungsenergien und der Abschätzung für die Rotation der  $C_\zeta - N_\eta$  Bindungen ergibt sich, dass eine Konformationsänderung kein limitierender Faktor für die Bindung von aDMA/sDMA-Proteinmotiven an Tudor-Proteindomänen ist.

## Abstract

Symmetrically and anti-symmetrically dimethylated arginine (sDMA and aDMA) are known to bind to Tudor domains. Tudor domain functionality is believed to depend on sDMA and sDMA modification. Crystal structures have shown binding of sDMA to be dependent on the conformation of the terminal methyl groups.

In this project the barrier of rotation around C-N bonds inside the guanidino system of sDMA and aDMA have been investigated. Rotation around the  $C_\zeta - N_\epsilon$  was investigated and found to be around  $12 \text{ kcal mol}^{-1}$ , but dependent on used solvent and counter ion. It has been concluded that the activation energy of  $C_\zeta - N_\eta$  bond rotation has to be very low because there was no rotational barrier of the  $C_\zeta - N_\eta$  bond visible down to 200 K in the taken NMR spectra. The activation energy of  $C_\zeta - N_\epsilon$  bond rotation for aDMA using HCl as a counter ion and methanol- $d_3$  as a solvent has been found to be  $8.9 \pm 0.9 \text{ kcal mol}^{-1}$ . Therefore it is concluded that conformational exchange of the guanidino methyl groups does not pose a limiting factor to binding of sDMA or aDMA motif containing proteins to Tudor domains.

# Contents

|          |  |           |
|----------|--|-----------|
| <b>1</b> | <b>Introduction</b>  | <b>2</b>  |
| <b>2</b> | <b>Theoretical background</b>  | <b>5</b>  |
| 2.1      | Nuclear Magnetic Resonance (NMR) . . . . .                                   | 5         |
| 2.2      | Chemical shift . . . . .   | 5         |
| 2.3      | Dynamic NMR . . . . .  | 6         |
| 2.3.1    | Classical method . . . . .   | 8         |
| 2.3.2    | Computational method . . . . .   | 8         |
| 2.4      | Data analysis . . . . .  | 10        |
| <b>3</b> | <b>Introduction to DMA</b>   | <b>14</b> |
| 3.1      | General description . . . . .  | 14        |
| 3.2      | ADMA . . . . .   | 14        |
| 3.3      | SDMA . . . . .   | 15        |
| 3.4      | Binding of sDMA and aDMA . . . . .   | 16        |
| <b>4</b> | <b>Experimental Section</b>  | <b>18</b> |
| <b>5</b> | <b>Main section</b>  | <b>20</b> |
| 5.1      | Measurements . . . . .   | 20        |
| 5.2      | Investigation of sDMA . . . . .  | 25        |
| 5.2.1    | Error estimation . . . . .   | 31        |
| 5.2.2    | Comparison of results with classical line shape analysis . .                 | 34        |
| 5.2.3    | Investigation of solvent influence on the activation energy                  | 36        |
| 5.2.4    | Investigation of counter ion influence on the activation<br>energy . . . . . | 37        |
| 5.3      | Examination of aDMA data . . . . .   | 40        |
| <b>6</b> | <b>Summary</b>   | <b>44</b> |
| <b>7</b> | <b>Appendix</b>  | <b>45</b> |
|          | List of figures . . . . .  | 45        |
|          | List of tables . . . . .   | 49        |
|          | List of abbreviations . . . . .  | 51        |

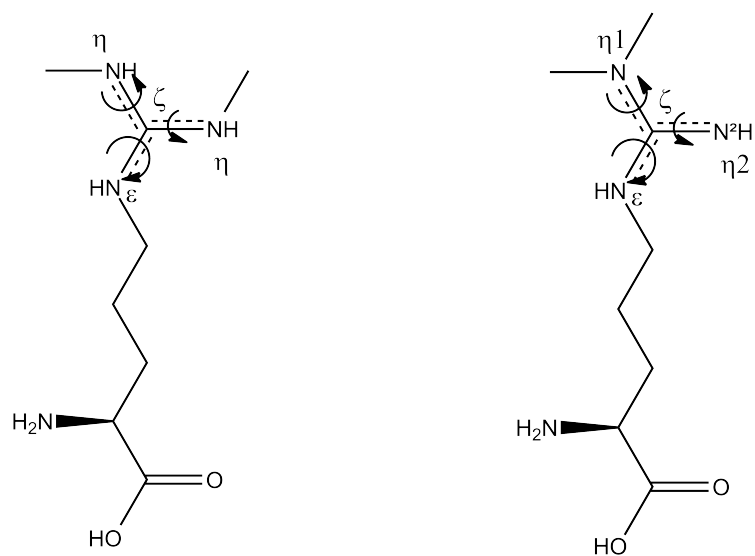
# 1 Introduction

The structure and dynamics of biological molecules and proteins play an important role in their functional behaviour. Therefore determination of conformation and further structural analysis are important to fully understand a molecule's application. Since many molecules are only biologically active in a distinct conformation, it is also important to find out the molecular dynamics of the given system in order to determine kinetic effects on chemical or physical reactions the system undergoes.

In order to derive structural information about the molecule there are different computational and experimental approaches. Computational approaches possess the disadvantage that it is very difficult to perfectly model the system which is physically present. Large effort has to be devoted to account for charges, solvent influence and chemical exchange and cannot resemble the actual system as close as experiments. To analyse conformational changes one has to choose a method which operates on the time scale and the size scale the change is taking place in. Nuclear Magnetic Resonance (NMR) spectroscopy operates on the time scale of micro to milliseconds which is suitable for the energy barriers around 5-26 kcal mole<sup>-1</sup>.<sup>[1]</sup> Rotational barriers like the one at hand have been reported to be within this value.

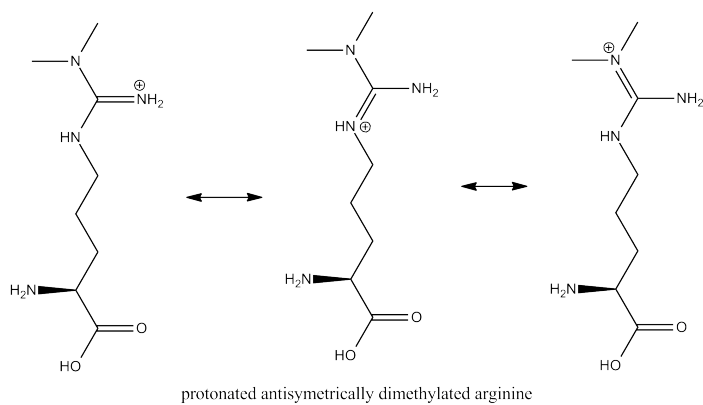
For analysing changes to small systems like the dimethylated arginine (DMA) system at hand in a liquid environment, it is favourable to choose magnetic resonance spectroscopy rather than optical spectroscopy. NMR enables more precise temperature control and better accuracy in determined rate constant, thus enabling a more precise determination of activation energies. In this experiment NMR spectroscopy methods will be utilised to study the molecular dynamics of an arginine system in aqueous solution.

In this experiment the barrier of rotation about partial double bonds in the guanidino like system of DMA shall be analysed using NMR spectroscopy. Rotation about  $C_\zeta - N_\eta$  and  $C_\zeta - N_\epsilon$  bonds shall be analysed as depicted in Scheme 1.1. For rotation in aDMA there are three different rotations observable as there is one about the  $C_\zeta - N_\epsilon$  bond as well as two distinct ones around  $C_\zeta - N_\eta^1$  and  $C_\zeta - N_\eta^2$  (Scheme 1.1). In sDMA both  $C_\zeta - N_\eta^1$  bond rotations are very similar (Scheme 1.1):

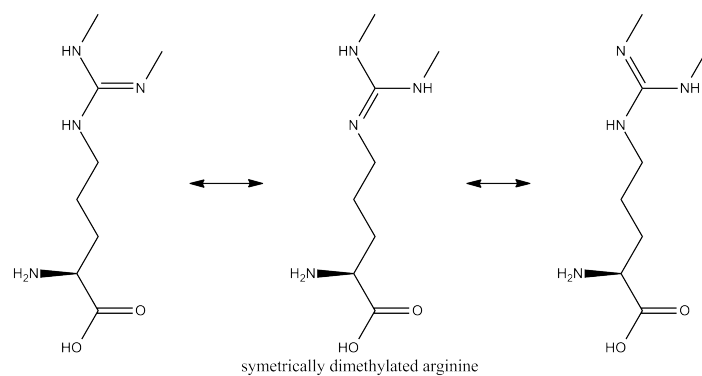


**Scheme 1.1** – Examined bond rotations of sDMA and aDMA

The partial double bond character of aDMA and sDMA is best illustrated by their corresponding resonance structures.



**Scheme 1.2** – Resonance structures of aDMA



**Scheme 1.3** – Resonance structures of sDMA

The aim of this bond rotation analysis is to determine if conformational exchange might be a limiting factor to sDMA binding in Tudor domains.

## 2 Theoretical background

### 2.1 Nuclear Magnetic Resonance (NMR)

The most popular magnetic resonance technique is NMR. NMR is widely used with organic, inorganic chemists and biochemists for structural determination and substance identification as well as sample analysis. NMR spectroscopy is based on the Zeeman effect. In an external field the energy of possible quantum states for a magnetic dipole is given according to 2.1.1

$$E = -\vec{\mu}_N * J_Z * |\vec{B}| = -\gamma_N * \frac{h}{2\pi} * j_Z * |\vec{B}| \quad (2.1.1)$$

where  $\vec{\mu}_N$  is the nuclear magneton,  $J_Z$  is the angular momentum quantum number and  $|\vec{B}|$  is the magnetic field. Since there are only two possible orientations  $|\alpha\rangle$  and  $|\beta\rangle$  for a spin 1/2 nucleus which correspond to quantum number  $j_z$  values of +0.5 and -0.5 accordingly the energy of transition between two electronic states is:

$$\Delta E = -g_N * \mu_N * |\vec{B}| = -\gamma_N * \frac{h}{2\pi} * |\vec{B}| \quad (2.1.2)$$

With the help of NMR one can measure these energy transitions using radio frequencies. The value for  $g_N$ , which is the Lande g-factor, varies for different nuclei and does not possess a unit. In NMR the gyromagnetic ratio  $\gamma$  is commonly used. For the ones used in this experiment the values are: <sup>[2]</sup> The data is collected

**Table 2.1** – Gyromagnetic ratios for nuclei observed during experiments

| nucleus/Isotope | I (spin) | relative abundance [%] | $\gamma$ [MHz T <sup>-1</sup> ] |
|-----------------|----------|------------------------|---------------------------------|
| <sup>1</sup> H  | 0.5      | 99.99                  | 42.576                          |
| <sup>13</sup> C | 0.5      | 1.10                   | 10.708                          |
| <sup>15</sup> N | 0.5      | 0.37                   | 4.3172                          |

by measuring the free induction decay of spin stated that are excited using pulse sequences.

### 2.2 Chemical shift

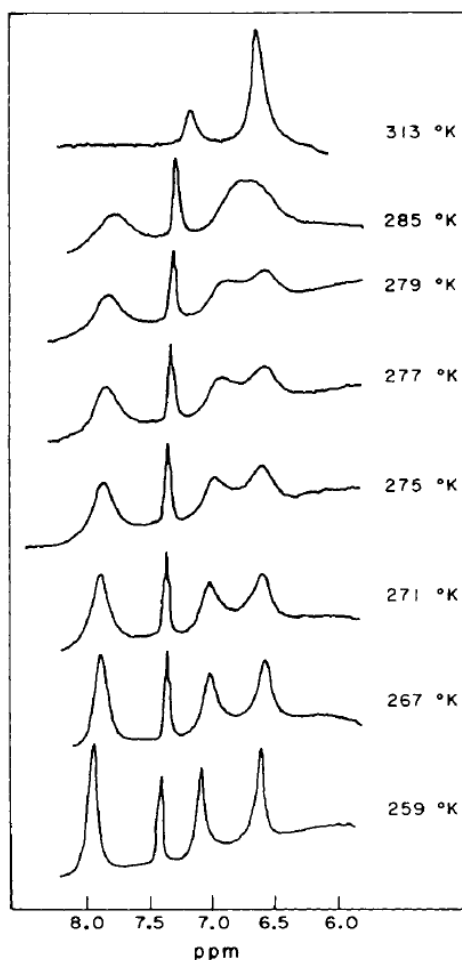
According to the rules stated so far there would be only one line visible in a NMR spectrum. Hence there has to be another important underlying effect for

NMR spectroscopy. As long as a molecule is inside a magnetic field, its electronic wave functions induce another magnetic field which is oriented anti-parallel to the outer magnetic field. This induced magnetic field  $\vec{B}_{int}$  induces a so-called chemical shift on the obtained resonance frequencies. Chemical shift is not an absolute value but can only be given in reference to existing systems. For  $^1\text{H}$  and  $^{13}\text{C}$  spectra the chemical shift is given in relation to tetramethylsilane(TMS), whereas  $^{15}\text{N}$  is calibrated relative to liquid ammonia. Chemical shift in respect to TMS and between peaks are given in ppm while coupling constants are given in Hz.

## 2.3 Dynamic NMR

Dynamic NMR(DNMR) is a method to analyse exchange processes on an atomic level. Examples of typical DNMR models are rotation around partial double bonds, ring inversions, ligand reorganisation and pseudo-rotations<sup>[1,3-8]</sup>. DNMR analysis is based on line broadening effects the signals experience when undergoing exchange processes. In this case rotation around partial double bonds shall be studied. Chemical exchange and therefore line broadening is a temperature dependent process.

As the temperature is increased during the experiments signals undergoing exchange start to affect each other as the reaction rate occurs on a detectable NMR time scale. Firstly in the slow exchange regime the signals start to broaden with increasing temperature, then these move towards one another and overlap at the point of coalescence. After reaching the coalescence point the signal sharpens and approaches natural line width, which is due to spin-spin and spin-lattice relaxation. This signal sharpening is due to the exchange time scale becoming significantly shorter than the measurement time, therefore causing the signal to appear as though it was just one. In this fast exchange regime the signal still consists of two independent resonances which are averaged over the NMR time scale. Scheme 2.1 illustrates this for the example of arginine.



**Scheme 2.1** – 270 MHz proton NMR of L-arginine HCl in 7 mM sodium acetate and 3.5 mM Na<sub>2</sub>EDTA and 30% CD<sub>3</sub>OH at pH 5.3; arginine concentration is 70 mM; image taken from<sup>[9]</sup>

In order to be able to perform DNMR analysis a series of requirements has to be met to obtain decent data. The data set needed to perform proper DNMR analysis has to contain a temperature series of comparable spectra preferably including the coalescence temperature. Since processes studied by DNMR are temperature dependent the temperature at which spectra are taken has to be calibrated in order to avoid systematic error. This can for example be assured by applying a temperature calibration to the used spectrometer with a chemical shift sample. Chemical shift samples are samples that show a distinct chemical shift or shift differences at each possible temperature. Moreover it is important that only processes which are at equilibrium can be investigated. There has to be a significant amount of both species present at equilibrium ( $\gg 1\%$ ) which has to be the case here since both examined conformations are of similar energy. There are two different ways of studying DNMR spectra: the 'classical method' and computational methods. In this project both are used to acquire reaction

rates.

### 2.3.1 Classical method

The classical method only requires line broadening information that can be easily obtained by the given spectra. Line broadening can be read out of the spectra by measuring the full width at half-maximum height (FWHM). Reaction rates  $k$  can be calculated using the following equations<sup>[10]</sup>:

for uncoupled nuclei at coalescence

$$k[\text{Hz}] = \frac{\pi}{\sqrt{2}} * \nu_{AB} = 2.22 * \nu_{AB} \quad (2.3.1)$$

for signal broadening after coalescence (higher temperature)

$$k = \frac{\pi \nu_{AB}^2}{2(\Delta\nu - \Delta\nu_{ref})} \quad (2.3.2)$$

for signal broadening before coalescence

$$k = \pi(\Delta\nu - \Delta\nu_{ref}) \quad (2.3.3)$$

where  $\nu_{AB}$  is the chemical shift in (Hz) between the observed signals A and B,  $\Delta\nu$  is the measured FWHM and  $\Delta\nu_{ref}$  is the FWHM of a reference peak which does not undergo exchange. The advantage of this method is that it has been tested and found to give a good estimate for the rate constant and the corresponding energy of activation. It is also very quick and easy and can be used to compare with computational data. A disadvantage of this method is its higher inaccuracy compared to the computational method especially around the point of coalescence, where noise has a high influence on the spectrum quality. Furthermore it does not account properly for varying shim quality, line temperature dependent line broadening and further spectral properties that can change between measurements. Especially for very low temperatures perfect tuning and matching is not possible any longer which results in loss of spectral quality.

### 2.3.2 Computational method

In contrast to the classical method, in computational methods like the TOPSPIN DNMR module used in this case the entire line shape is fitted using variables for peak position and intensity, line broadening, exchange rate and J-coupling constants. These simulations are based on Bloch Equations which can be used for uncoupled systems, Monte-Carlo methods or density matrix calculations (DMC)<sup>[11]</sup>.

The programme at hand used average DMC and does parameter optimization iteratively<sup>[4,6,12]</sup>.

As chemical exchange can be interpreted as a chemical reaction the reaction speed is given by

$$k = \sum_B \frac{1}{\nu_B} \frac{d[B]}{dt} \quad (2.3.4)$$

where B is the reacting compound and  $\nu_B$  is the stoichiometric coefficient of each product. Since the rotational reaction does not change the molecule there is only one product, therefore B and  $\nu_B$  become 1. This simplifies 2.3.4 to:

$$k = \frac{1}{\nu_B} \frac{d[B]}{dt} \quad (2.3.5)$$

thus the life time  $\tau$  being:

$$\tau = \frac{\nu_B}{\frac{d[B]}{dt}} \quad (2.3.6)$$

Since the programme works on DMC chemical exchange has to be applied to the system using a matrix model. As two systems are interchanged within chemical exchange the basis functions for each nucleus involved in the specific reaction interchange. For the simplest assumption of just two nuclei interacting plus another one for line shape comparison, and one basis function each, the basis set matrix M before interchange becomes:

$$M^{before} = \begin{bmatrix} \Psi_1 \\ \Psi_2 \\ \Psi_3 \end{bmatrix} = \begin{bmatrix} \psi_{11} * \psi_{12} * \psi_{13} \\ \psi_{21} * \psi_{22} * \psi_{23} \\ \psi_{31} * \psi_{32} * \psi_{33} \end{bmatrix} \quad (2.3.7)$$

After interchange of Nuclei 1 and 2 the result is

$$M^{after} = \begin{bmatrix} \Psi_1 \\ \Psi_2 \\ \Psi_3 \end{bmatrix} = \begin{bmatrix} \psi_{12} * \psi_{11} * \psi_{13} \\ \psi_{22} * \psi_{21} * \psi_{23} \\ \psi_{32} * \psi_{31} * \psi_{33} \end{bmatrix} \quad (2.3.8)$$

This interchange of two indices resembles the permutation of two nuclei, leading to a simple exchange matrix X whose elements are

$$X_{mn} = \langle \Psi_n^{before} | \Psi_m^{after} \rangle \quad (2.3.9)$$

m and n indicating row and column matrix indices respectively. Fitting is then done by calculating the overlap between signal intensities of simulated and experimental spectra. The program gives the following formula for fit quality:

$$FIT = 100 * \left( 1 - \frac{\sum_{\nu} |Y_{sim}(\nu) - Y_{exp}(\nu)|}{2 \sum_{\nu} Y_{exp}(\nu)} \right) \quad (2.3.10)$$

with  $Y_{sim}(\nu)$  being the simulated and  $Y_{exp}(\nu)$  being the experimental point at frequency  $\nu$ <sup>[13]</sup>. Only fits with value larger than 90 have been accepted for data analysis.

This method comes with more parameters and options. Since line broadening and rate constant changes have similar effects on exchanging peaks, one has to obtain values for natural line broadening by comparison with other peaks in the spectrum that behave similarly (experience comparable line broadening due to neighbouring protons, chemical environment), which cannot always be achieved. If one does find such a peak this method provides a very good estimate for temperature dependent line broadening effects like solvent viscosity. Furthermore peak position and reaction rate affect each other since peaks of smaller separation also show coalescence at lower temperatures. To manage these problems one can either get an estimate of line broadening and chemical shift between peaks below coalescence from comparison of the analysed peaks with spectra of known chemical exchange (either complete or virtually no exchange over the NMR time scale) or rely on comparison with other signals within the analysed spectra.

One large source of error of this method is that peak separation occurs below coalescence but also plays an important role far above the coalescence when simulating spectra. The chemical shift between both peaks seems to change below coalescence in some spectra even though peak separation should be unchanging below coalescence temperature, so there is no proper estimation of chemical shift possible above coalescence. Comparison shows that results for different variable values are similar but not identical and account for uncertainties even when analysing the full line spectra. Errors caused by uncertainties in respect to variable parameters result in much larger errors than any other error (e.g. from noise) and can therefore be used as an indication for the error size.

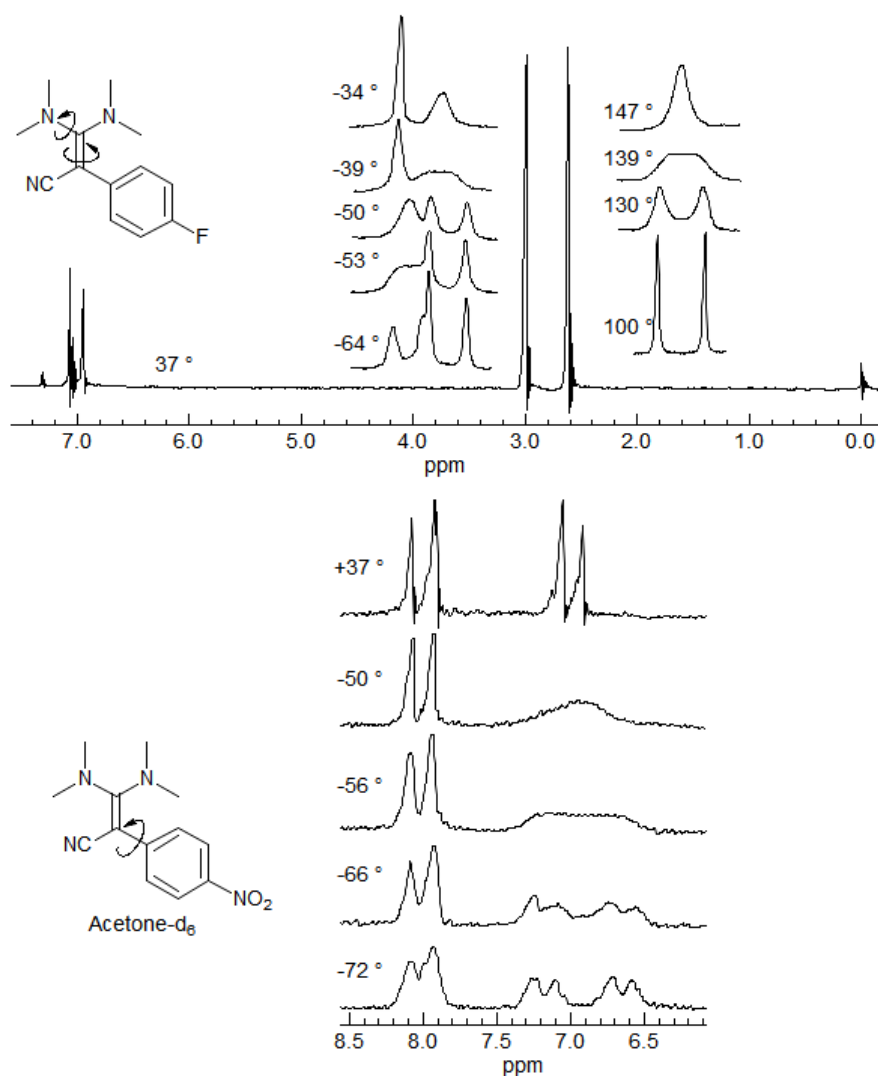
Overall advantages of this method are a more precise value for a rate constant especially when fitting data around the coalescence point and the ability to account for random error of single experiments. One disadvantage of this method is that the formula implemented for rate constant calculation is not known. Further details on the program are available from the BRUKER TOPSPIN3.2 DNMR manual<sup>[13]</sup>.

## 2.4 Data analysis

Firstly a rough estimate of the activation energy can be gained by comparison with known data (e.g from Hans Reich's DNMR web page)<sup>[1]</sup>.

**Table 8.3.1**  $\Delta G^\ddagger$  (kcal/mole) as a Function of Peak Separation and Temperature

| $\nu_{AB}$ | $T_c \rightarrow$ | 200  | 150  | 100  | 50   | 0    | -50  | -100 | -150 | -200 |
|------------|-------------------|------|------|------|------|------|------|------|------|------|
| 5 Hz       |                   | 25.9 | 23.0 | 20.2 | 17.4 | 14.6 | 11.9 | 9.1  | 6.4  | 3.7  |
| 50 Hz      |                   | 23.7 | 21.1 | 18.5 | 15.9 | 13.4 | 10.8 | 8.3  | 5.8  | 3.4  |
| 500 Hz     |                   | 21.5 | 19.2 | 16.8 | 14.5 | 12.1 | 9.8  | 7.5  | 5.3  | 3.1  |
| 5000 Hz    |                   | 19.4 | 17.2 | 15.1 | 13.0 | 10.9 | 8.8  | 6.7  | 4.7  | 2.7  |

**Scheme 2.2** – Activation energy as a function of peak separation and temperature<sup>[1]</sup>**Scheme 2.3** – Example for DNMR measurements for rotation about a partial double bond<sup>[1]</sup>

After rate constant analysis further data processing is necessary to determine activation energy, transition state enthalpy and entropy. Reaction rate and

## THEORETICAL BACKGROUND

---

activation energy are set into relation by the Arrhenius equation:

$$k = Ae^{\frac{-E_a}{RT}} \quad (2.4.1)$$

where A is the pre-exponential factor,  $E_a$  is the activation energy, R is the universal gas constant  $\frac{1.986kcal}{K \cdot mol}$ . Rearranging the equation gives:

$$\ln(k) = \ln(A) - \frac{-E_a}{RT} \quad (2.4.2)$$

The activation energy for each reaction can be obtained using an Arrhenius plot. By plotting  $\ln(k)$  against  $(1/T)$  a graph with a slope of  $-\frac{E_a}{R}$  and a y-axis intercept of  $k_0$  is drawn. The slope is calculated using linear regression, which tries to fit all values in order to reach a minimum in standard deviation. The pre-exponential factor shall no longer be of interest but the energy of activation which can be acquired by multiplying the slope with -R.

$$k = -m * R \quad (2.4.3)$$

In an equal fashion values for the change in enthalpy and entropy can be obtained using a different form of the Arrhenius equation:

$$k = \frac{k_B T}{h} \frac{RT}{p_0}^{m-1} e^{\frac{-\Delta G^\ddagger}{RT}} \quad (2.4.4)$$

Substituting Gibbs law of free energy

$$\Delta G = \Delta H - T\Delta S \quad (2.4.5)$$

2.4.5 becomes

$$k = \frac{k_B T}{h} \left( \frac{RT}{p_0} \right)^{m-1} e^{\frac{-\Delta H^\ddagger}{RT}} e^{\frac{\Delta S^\ddagger}{R}} \quad (2.4.6)$$

where  $\Delta G$  is Gibbs free enthalpy,  $\Delta H$  is the change in enthalpy and  $\Delta S$  is the change in entropy, while  $^\ddagger$  indicates a transition state. The reaction order is given by  $m$  while  $p_0$  is ambient pressure. For the transition state  $\Delta G^\ddagger$  is the same as the activation energy. The reaction order of rotation around a double bond is 1, simplifying 2.4.6 to:

$$k = \frac{k_B T}{h} e^{\frac{-\Delta H^\ddagger}{RT}} e^{\frac{\Delta S^\ddagger}{R}} \quad (2.4.7)$$

Dividing by temperature and taking the natural logarithm of both sides gives:

$$\ln\left(\frac{k}{T}\right) = -\frac{\Delta H^\ddagger}{R} * \frac{1}{T} + \ln\left(\frac{k_B}{h}\right) + \frac{\Delta S^\ddagger}{R} \quad (2.4.8)$$

Thus one can plot  $\ln\left(\frac{k}{T}\right)$  against  $\frac{1}{T}$  to get the enthalpy of activation state from the graph's slope and the entropy from the y-axis intercept. This gives further information about the reaction, but comes with greater uncertainty values<sup>[10]</sup>. The activation energy of a rotational barrier determines the life time of the corresponding rotational state. Being able to give an estimate for the life time

of each rotational state is essential for determining if rotation has an effect on DMA binding. A good approximation is given by 2.4.9:

$$\ln(k) = \ln\left(\frac{k_B}{h}\right) + \ln(T) - \frac{\Delta G^\ddagger}{RT} \quad (2.4.9)$$

and

$$t_{1/2} = \frac{\ln(2)}{k} \quad (2.4.10)$$

yields

$$t_{1/2} = \frac{\ln(2)}{\ln\left(\frac{k_B}{h}\right) + \ln(T) - \frac{\Delta G^\ddagger}{RT}} \quad (2.4.11)$$

For examples of DNMR spectral analysis see references<sup>[1]</sup>.

## 3 Introduction to DMA

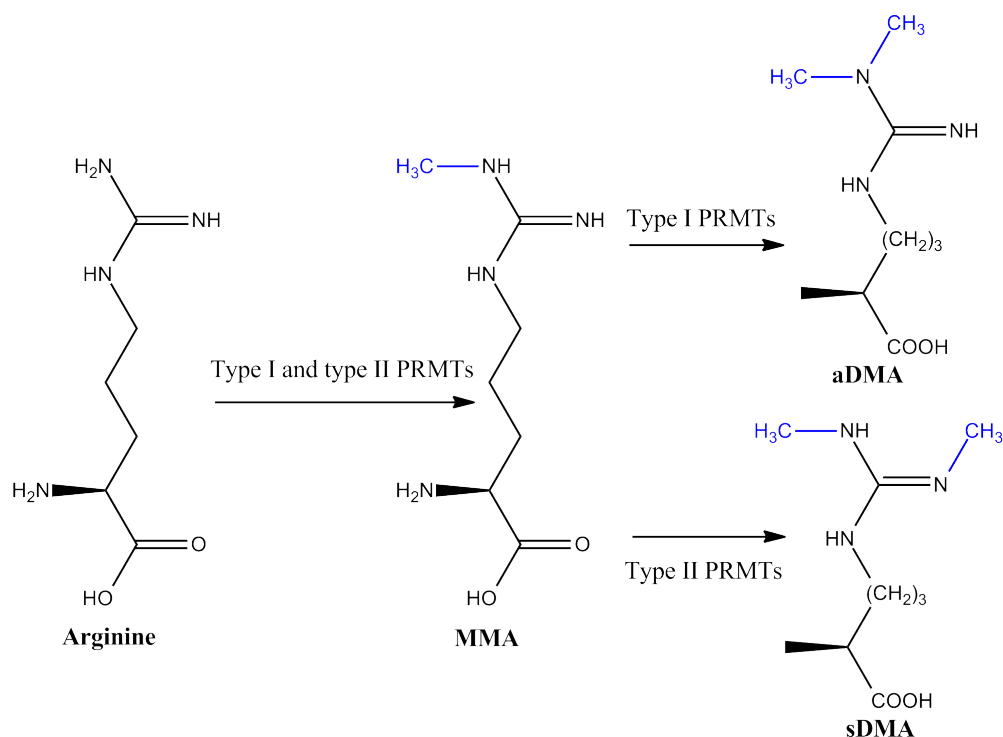
### 3.1 General description

Methylation of arginine residues is one among a variety of post-translational modifications (PTMs). There are three different kinds of arginine methylation currently known to naturally occur in biological systems. These three are mono methylated arginine (MMA), symmetrically methylated arginine (sDMA) and anti-symmetrically methylated arginine (aDMA), where MMA is believed to only exist as an intermediate product to dimethylation<sup>[14]</sup>. Symmetrically dimethylated arginine is produced by protein arginine methylation transferase type II (PRMT5, PRMT7) which places two methyl groups on each of the terminal nitrogen atoms of the guanidino group whereas aDMA is created by type I PRMT (PRMT1, PRMT4, PRMT6, PRMT8) by replacing two hydrogen atoms with two methyl groups on the same terminal nitrogen atom of the guanidino group<sup>[15]</sup>. Within the methylation process methyl groups are donated by S-adenosyl methionine to L-arginine in proteins. The methylated arginine compounds are later released during proteolysis.

These modifications have been linked to cellular processes such as trafficking, signal transduction, RNA processing and gametogenesis<sup>[16][17]</sup>. Arginine methylation is known to be recognized by a variety of Tudor domain containing proteins. One group of special interest is the survival motor neuron protein (SMN) as well as the related splicing factor 30 (SPF30) which specialise in the recognition of sDMA. SMN and SPF30 are important for the assembly of uridine-rich small nuclear ribonucleoprotein complexes<sup>[18-20]</sup>, cellular trafficking<sup>[21]</sup> and in pre-mRNA splicing<sup>[22,23]</sup>. Also lack of SMN presence is one cause of spinal muscular atrophy (SMA).

### 3.2 ADMA

Asymmetrically methylated arginine is also recognized by Tudor domains, like the aDMA modulated human transcription elongation factor CA150<sup>[24]</sup>. In comparison to sDMA it shows lower binding affinity, in comparison to MMA higher binding affinity to Tudor domains. Generally binding of aDMA works via the same mechanisms as for sDMA, but always showing slightly lower affinities<sup>[?]</sup>. Further aDMA plays an important role in regulating the activity of NO synthesis.



**Scheme 3.1** – Modification of arginine to sDMA and aDMA by PRMTs

Higher aDMA or lower L-arginine levels cause inhibition of NO synthesis which is necessary for vasodilation.<sup>[25]</sup> Nitrogen monoxide also inhibits cell proliferation, aggregation of thrombocytes, monocytes adhesion and eliminates free radicals<sup>[26-28]</sup>. Therefore high aDMA levels are linked to a variety of diseases or health conditions like cardiovascular disease (especially hypertension), metabolic disease, diabetes mellitus and chronic kidney disease<sup>[27,29]</sup>.

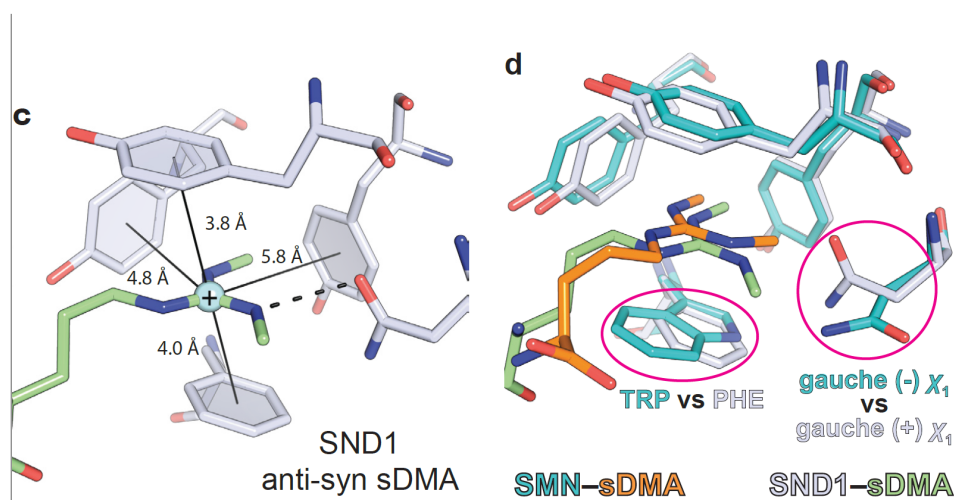
### 3.3 SDMA

It is believed that the interaction between sDMA and Tudor domains takes place according to a reader-writer-eraser model although the presence of an eraser has not been proven yet<sup>[30,31]</sup>. Binding affinity of Tudor domains to arginine residues is significantly increased by arginine methylation. It has also been proven that SMN to Sm interaction can be inhibited by specific sDMA methylation<sup>[32,33]</sup>. In addition reports show that symmetrically dimethylated peptides are able to pull down SMN from HeLa extracts [5s]. Furthermore interaction between P-element induced wimpy testis proteins (PIWI) and Tudor domains is believed to be regulated by arginine methylation<sup>[14]</sup>. These lines of evidence show the importance of sDMA modification to cellular processes, since abolishing of operativeness of Tudor domains or PRMTs has a large impact on proper piRNA biogenesis and on piRNA profiles. These effects include “mislocalisation of PIWI

proteins and severely reduces levels of total piRNA in testes” [14,34,35].

### 3.4 Binding of sDMA and aDMA

Binding of sDMA by Tudor domains is done by the accommodation of sDMA into an aromatic cage which does not alter its conformation due to binding of the sDMA motif<sup>[14]</sup>. This aromatic cage consists of a tryptophan and a tyrosine which are assembled parallel to the plane in which the guanidino system coordinated. The aromatic cage is completed by another tyrosine residue and a fourth inconsistent residue. The guanidino system possesses a partial positive charge on its centre carbon atom. Binding is achieved by cation- $\pi$  interaction. Studies have shown that the sDMA is stacked at van der Waals distance to the face of the parallel orientated aromatic residues of the aromatic cage. Additional stabilisation is granted to the system due to cation- $\pi$  interaction in a T-shaped geometry with the orthogonally orientated aromatic residues<sup>[36,37]</sup>.



**Scheme 3.2** – Crystal structure of aromatic pocket taken from<sup>[15]</sup>

Positioning of aDMA does not appear to be optimal as the guanidino group was not placed perfectly parallel to the aromatic ring  $\pi$  electron cloud, resulting in lower binding affinity. The DMA methyl groups provide a steric effect that guides the guanidino group in respect to the aromatic cage, enabling the binding pocket to distinguish between DMA and MMA or arginine compounds. Furthermore

studies have shown that a hydrogen bond triangle between Tyr127, Glu134 and Glu136 of the Tudor domain significantly increased the binding affinity for DMA<sup>[15]</sup>.

As the conformation in which DMA is bound inside the aromatic cage seems to have an effect on the binding affinity, different rotameric states and conformations are imaginable for binding. Different conformations of sDMA have been observed for SMN and extended Tudor domains (here: SND1). Binding to SMN the cavity was found to obtain an anti-syn conformation while the asparagine is in a gauche(-) $\chi_1$  rotameric state whereas the sDMA residue was accommodated in an anti-anti conformation with asparagine being in the gauche(+) $\chi_1$  rotameric state when binding to SND1.

Density function theory (DFT) calculations have shown that the energy difference between both conformations of sDMA is about 2.8 kcal mole<sup>-1</sup>. Furthermore it has been found that it is sterically impossible for the system to obtain a gauche(+) $\chi_1$  rotameric state while the cavity is in anti-syn conformation or to obtain a gauche(-) $\chi_1$  rotameric state while the cavity is in anti-anti conformation. Given these results one should investigate the barriers of rotation around the C-N bonds, especially the  $C_\zeta - N_\eta$  bond, of the guanidino system to find out if conformational inversion does have an influence on sDMA binding properties. A rigid steric conformation might result in additional barriers to sDMA binding<sup>[15]</sup>.

## 4 Experimental Section

All spectra were collected on a 600 MHz Avance Spectrometer from Bruker and analysed with the Topspin 3.2 programme. Topspin DNMR 1.1 was used for computational line shape fitting. Probe cooling was done passing nitrogen gas flow through a liquid  $N_2$  heat exchanger. The lowest measured sample temperature was reported as 200 K. Cooling beyond this temperature would require cooling by evaporating liquid nitrogen into the spectrometer. Temperature control is far more complicated using evaporating nitrogen as well as these low temperatures pose a danger to the spectrometer seals. With a home-built device (hot air blower with cardboard extension tube) shim-coil and seal temperature could be partially stabilised down to sample temperatures of about 230 K.

Further sample cooling should yield another point of coalescence. To achieve even lower temperatures one will have to make sure that the NMR spectrometer seals as well as the shim coils are sufficiently heated to ensure safety. Therefore modifications to the spectrometer have to be applied since externally heating the shim coils has shown to be non-sufficient to ensure no water condensation inside the spectrometer. Furthermore another solvent has to be chosen for the sample that remains liquid at such low temperatures. Methanol has a freezing point of 175 K and has been chosen as it is a good representative for a protic polar environment. For spectral recording different pulse programmes are used. The full pulse programmes can be found online<sup>[38] [39] [40] [41]</sup>.

All  $^1H$  spectra are recorded using a zero-go procedure, which acquires a simple 1 D spectra without decoupling using a 90 degree flip angle. Furthermore a zgpgw5 programme is run which records 1-D spectra with solvent signal suppression. The solvent signal suppression uses a W5 pulse train<sup>[38]</sup>. This pulse sequence uses a double WATERGATE suppression pulse. For decent solvent signal suppression the solvent signal position as well as the pulse phase has to be calibrated manually. The solvent viscosity decreases with temperature and the pulse becomes longer with increasing temperature. The results can be taken from the appendix, Table 7.1.

$^{13}C$  spectra were obtained using a zgdc30 programme. This programme acquires a standard  $^{13}C$  NMR spectrum with proton broad-band decoupling using a 30 degree flip angle. Decoupling simplifies the spectra showing only one line for each carbon atom rather than a multiplet due to scalar coupling with neighbouring  $^1H$  atoms<sup>[39]</sup>. During decoupling sequences there is a lot of energy applied to spins to keep them from relaxation into the ground state and build up scalar

---

couplings. Partial absorption of energy by the sample causes sample heating which is a disadvantage when performing temperature dependent analysis.

For  $^1H - ^{15}N$  HSQC and  $^1H - ^{13}C$  HSQC spectra different pulse programmes are used. All spectra for aDMA and sDMA with HCl as a counter ion were collected using the pulse programme hsqcetf3gp (HSQC phase sensitive Echo/Antiecho gradients with defined f3 channel, in this case  $^{15}N$ ). For  $^1H - ^{13}C$  HSQC spectra the f3-channel remains as defined by the spectrometer(hsqcetgp). This pulse programme is used for the acquisition of 2D-HSQC spectrum. Selection by echo-antiecho gradient only allows detection of direct  $^1H - ^{15}N$  signals while other signals are suppressed by the applied gradients<sup>[40]</sup>.

In order to analyse the sDMA HABS sample hsqcetf3gpnd pulse sequence was used. This gradient pulse sequence does not decouple (nd). Therefore there are two peaks visible for each  $^1H - ^{15}N$  cross peak. These mirror images can be overlaid exactly on half distance between their maxima to give rise to the actual physical cross peak. Working without decoupling reduces sample warming throughout the acquisition process. For  $^1H - ^{13}C$  HMBC hmbcgpndqf (HMBC gradient pulse low pass filter no decoupling) is used as a pulse programme<sup>[41]</sup>.

In all reported 2D-spectra the frequency range labelled f2 is the proton dimension.

## 5 Main section

To study the rotational barriers of sDMA and aDMA efficiently it is important to estimate their energy range. The guanidino system has been studied both theoretically as well as experimentally<sup>[42-44]</sup>. Furthermore there have been some studies on the rotational barrier of arginine<sup>[9,45]</sup>. These papers suggest that rotation around the  $C_\zeta - N_\eta$  bond as well as the  $C_\zeta - N_\eta$  bond are around 10-15  $kcal\ mol^{-1}$ . The general expectation is that rotation around the C-N bonds in the methylated guanidino system should have a slightly higher barrier than in arginine, due to the increased weight of the rotating group. Therefore a temperature range from 310 K downwards seems appropriate.

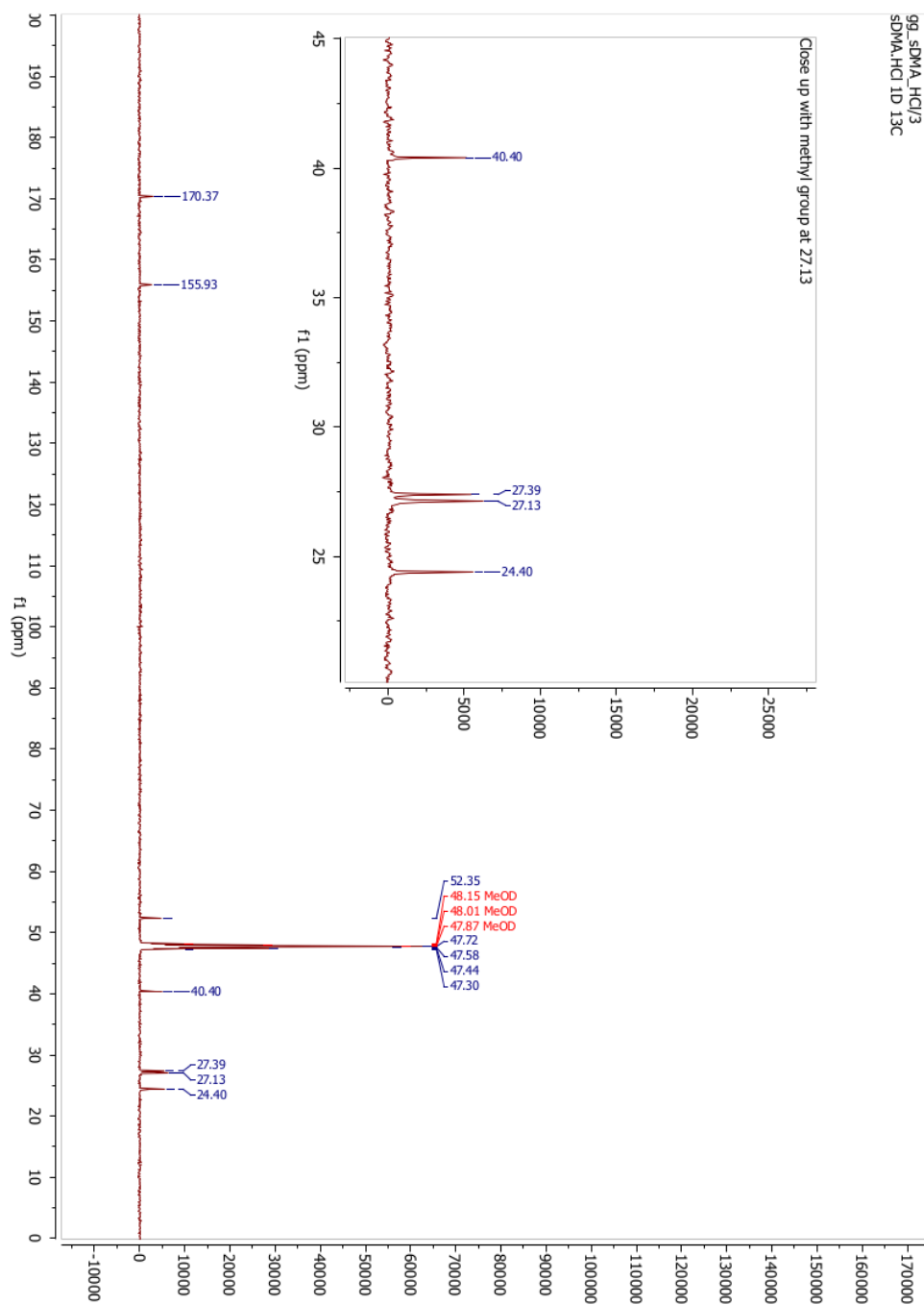
### 5.1 Measurements

At the beginning a temperature calibration has to be done over a temperature range from 200 K to 310 K using a 99.8% deuterated methanol sample of known temperature-chemical shift dependence. The temperature offset correlation between sensor and actual temperature was found to be linear and corrected for accordingly on the spectrometer. All measurements have been taken on the same spectrometer and the gained temperature calibration has been used throughout the experiments. This had to be done since switching samples is not possible at temperatures down to 200 K which would have been necessary due to the chosen calibration method. The temperature calibration is given in the appendix. For every temperature a  $^1H$  and  $^1H$ - $^{15}N$  HSQC spectrum has been recorded. For every measurement but the one with HABS as counter ion there have also been  $^{13}C$  spectra recorded. For general discussion  $^{13}C$  spectra shall be used, except for the sample containing HABS as a counter ion, for which those rows of a  $^1H$ - $^{15}N$  HSQC spectra containing information about the  $N_\eta$ -protons are used. In order to study different influences on the rotational barrier three samples containing sDMA have been prepared as well as one sample containing aDMA.

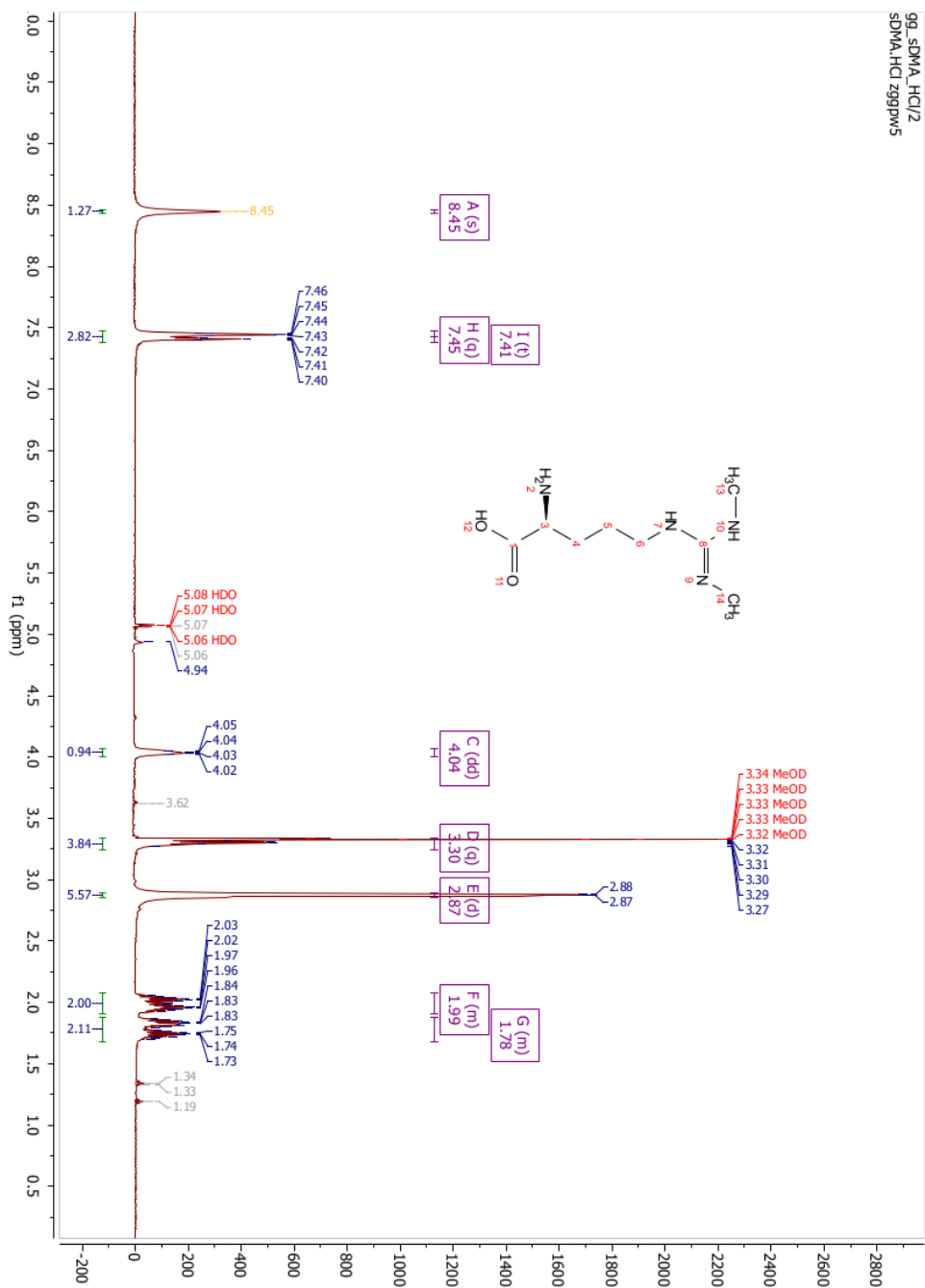
To determine if the rotational barrier is significantly larger than the estimated value spectra at 280 K and 310 K were recorded. A detailed description of peak assignment for different temperatures has been done in Table 7.3 and Table 7.2. As one can see from Scheme 5.1 there is only a single peak observable for every Carbon atom. The same observation is made in the  $^1H$  spectra, Scheme 5.3 and Scheme 5.3, indicating that there is no frozen rotation at this temperature.

Table 5.1 – sample setup

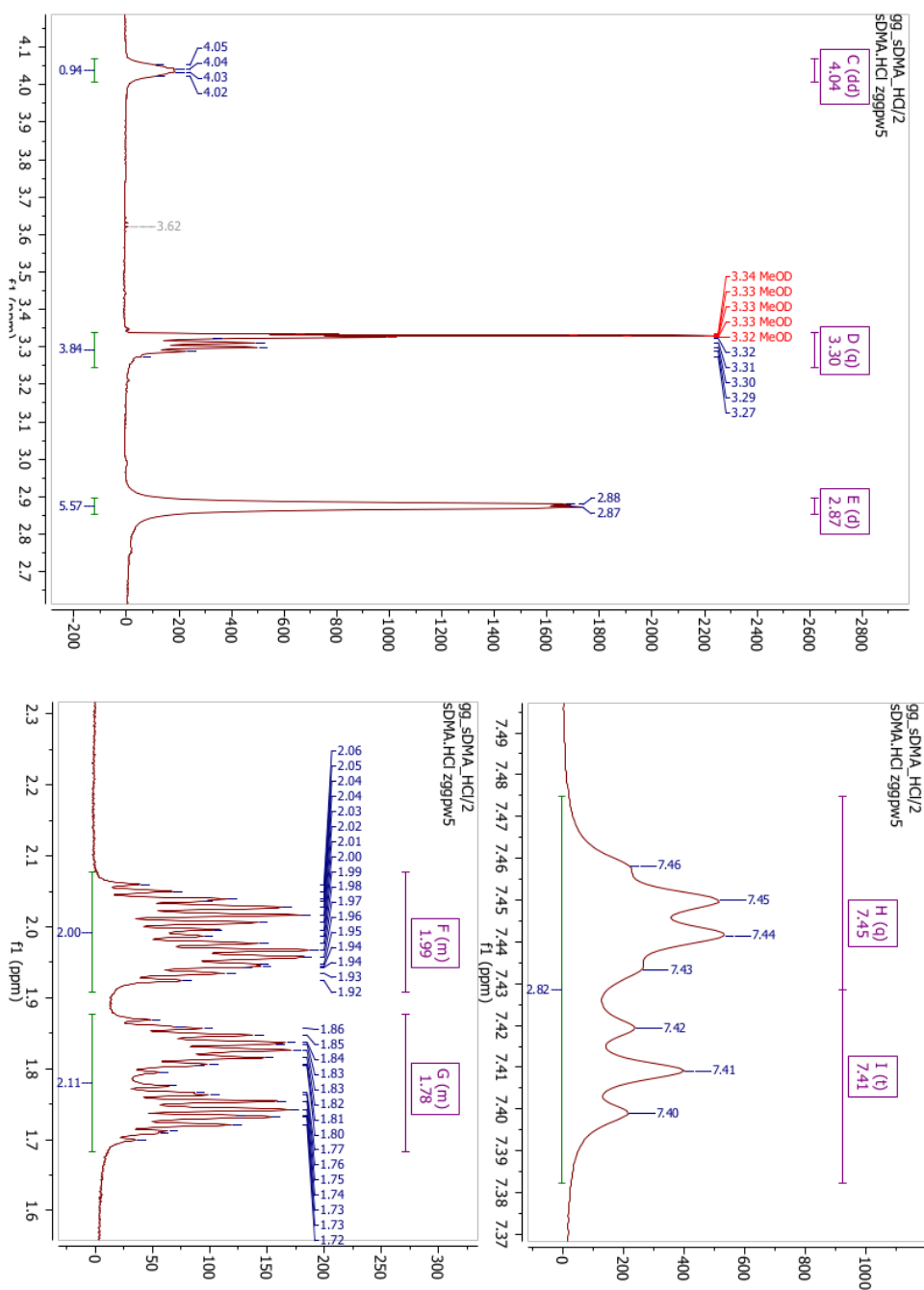
| arginine modification | amount used [mg] | counter ion | solvent       | solvent volume [ $\mu$ l] |
|-----------------------|------------------|-------------|---------------|---------------------------|
| sDMA                  | 9.4              | HCl         | $CD_3OH$      | 500                       |
| sDMA                  | 9.1              | HCl         | $CD_3OH/H_2O$ | 300/300                   |
| sDMA                  | unknown          | HABS        | DMSO/ $H_2O$  | both 50 vol %             |
| aDMA                  | 9.7              | HCl         | $CD_3OH$      | 500                       |

Scheme 5.1 –  $^{13}C$  spectrum of sDMA methanol- $d_3$  at 280K

MAIN SECTION



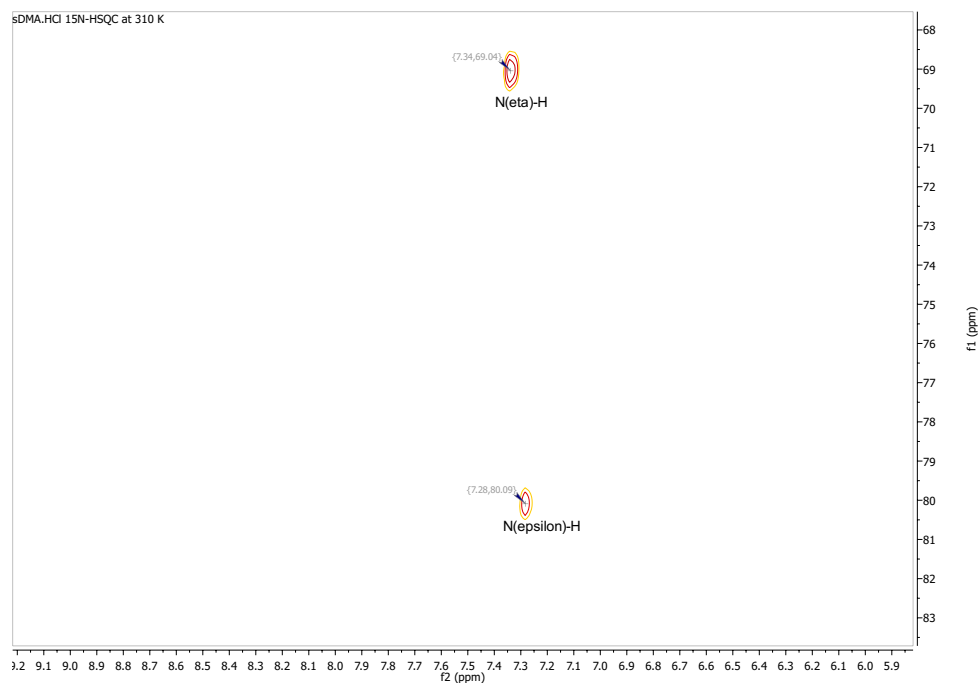
Scheme 5.2 –  $^1\text{H}$  spectrum of sDMA methanol- $\text{d}_3$  at 280K



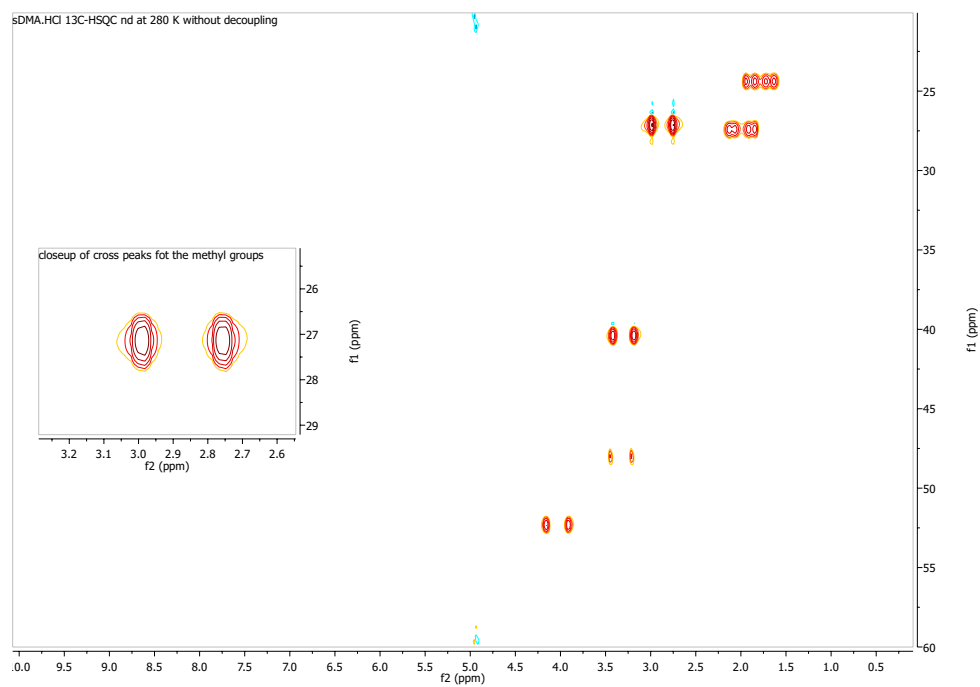
**Scheme 5.3** –  $^1\text{H}$  spectrum of sDMA methanol- $\text{d}_3$  at 280K showing close up of methyl peaks

To be entirely sure furthermore one  $^1\text{H}$ - $^{15}\text{N}$  HSQC and one  $^1\text{H}$ - $^{13}\text{C}$  HSQC were recorded. The possibility of overlapping peaks is ruled out, since there is only one peak observed for all six methyl protons in Scheme 5.5 and only one cross

peak observed for both  $N_\eta$  protons in Scheme 5.4.



Scheme 5.4 –  $^1\text{H}$ - $^{15}\text{N}$  spectrum of sDMA methanol- $\text{d}_3$  at 310K



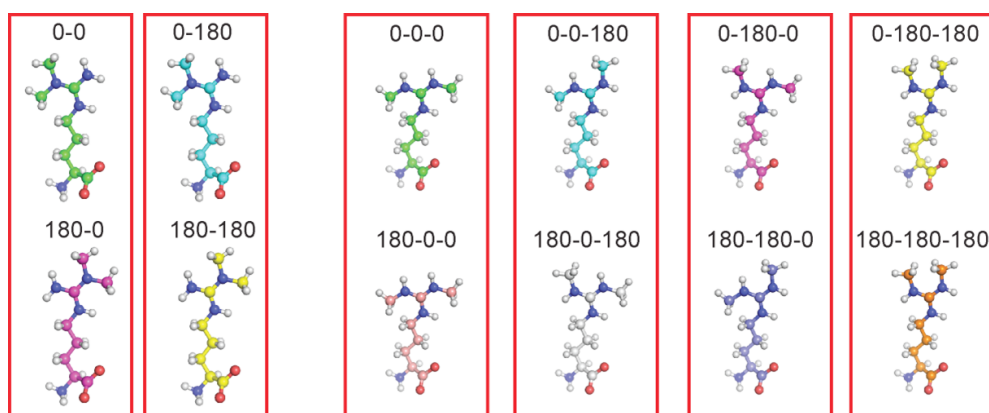
Scheme 5.5 –  $^1\text{H}$ - $^{13}\text{C}$  spectrum of sDMA methanol- $\text{d}_3$  at 280K

As one approaches the point of coalescence there should be observable line broadening and signal separation afterwards. The only case in which there is no line broadening is if both signals after coalescence are identical. It is reasonable to assume that this cannot be the case here since spectra of arginine have shown significantly separated peaks already<sup>[9,46]</sup>. One can also see that different conformations yield different electronic structures, therefore resulting in different chemical shifts.

## 5.2 Investigation of sDMA

First the solution containing HCl as a counter ion is measured. Starting at 310 K and cooling down the solution in 10 K steps there is only one coalescence observable, which occurs roughly at 265 K for the  $^1\text{H}$  and 263 K for the  $^{13}\text{C}$  spectra. The peak separation after the methyl peaks are base line separated is roughly 20.2 Hz for the  $^1\text{H}$  and 30 Hz for the  $^{13}\text{C}$  spectra. Usually as those observations describe the same chemical process they should have the same energy of activation. For a set energy of activation an increase in peak separation results in a higher coalescence temperature. This does not seem to be the case here. Since it is very unlikely that both spectra show different phenomena those influences are probably due to uncertainties between measurements and more importantly due to different line broadening. Since there was no line broadening applied to  $^1\text{H}$  spectra but 5 Hz line broadening applied to  $^{13}\text{C}$  the coalescence appears to be different, although it is not. Additional line broadening after Fourier transform makes the peaks broader and therefore look like they are coalescing a little earlier than they actually are. Taking these effects into account the coalescence temperature for looked at  $^{13}\text{C}$  spectra is around 5 K higher than predicted before, making it around 268 K.

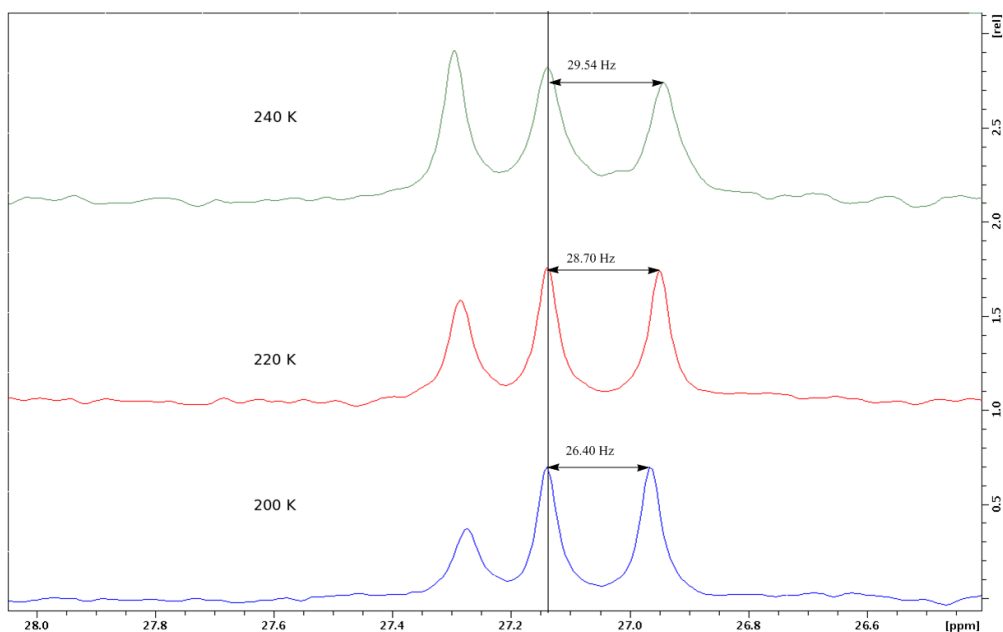
There are 8 different conformations of which 4 are equal for all bonds being rigid.



**Scheme 5.6** – Different possible conformations for aDMA(left) and sDMA(right) by courtesy of M. Sattler

For Scheme 5.6 the top and bottom row are of the same energy and therefore yield the same signals. Since there are two possible rotations within the guanidine system that could lead to peak separation, one has to determine which one was eventually observed. Several lines of evidence support the conclusion that the observed rotation is around the  $C_\zeta - N_\eta$  bond rather than the  $C_\zeta - N_\eta$  bond. Firstly peak multiplicity suggests that the observed rotation is around a  $C_\zeta - N_\eta$  partial double bond, since only two peaks are visible after coalescence. A frozen rotation around a  $C_\zeta - N_\eta$  bond partial double bond should lead into three distinguishable states with peak intensity 1:2:1. For rotation around the  $C_\zeta - N_\eta$  bond being frozen and around the  $C_\zeta - N_\eta$  bond still being active, conformations rotations 0-0-0, 0-180-180 and 0-0-180 or 0-180-0 corresponding to Scheme 5.6 are energetically different. Vice versa there are only two possible energetic states for each methyl group as rotation about the  $C_\zeta - N_\eta$  bond leads to an average value for every one methyl group of a guanidine imino side chain. The energy difference between each of those side chains remains detectable since they are located either in *cis* or *trans* conformation in respect to the  $N_\epsilon$ -proton via the  $C_\zeta - N_\eta$  partial double bond. Thus freezing out the rotation around the  $C_\zeta - N_\eta$  bond leads to a peak multiplicity of two.

After peaks that are undergoing chemical exchange have been separated completely, they should not move any more relative to one another whereas temperature induced chemical shifts can still occur. After the described peaks are separated they still seem to move, providing further uncertainties.



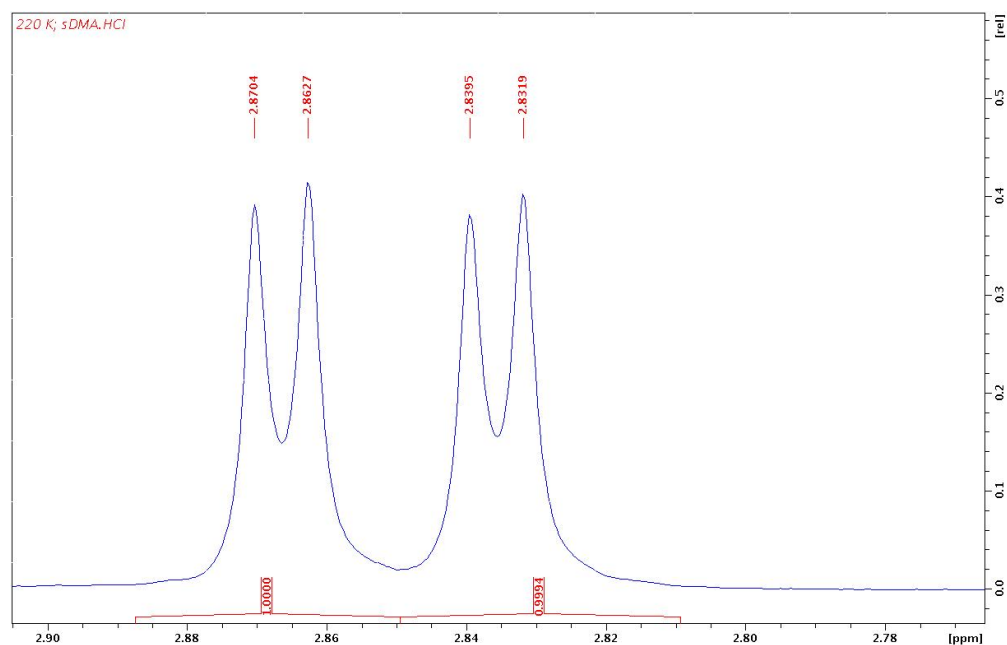
**Scheme 5.7** – Below coalescence the chemical shift between both methyl peaks is changing

So predicting the peak's theoretical position without above coalescence without

influences of chemical exchange is very difficult. Knowing a peak's theoretical position is very important since it is one of the variables in line shape analysing tools. As peaks move closer to one another the reaction rate for coalescence decreases. This thus leads to problems when trying to calculate the corresponding energy of activation. An increase in line separation could be explained if the peaks were moving further apart, as one could argue that chemical exchange is still significant for a longer period after coalescence.

The two methyl peaks seem to be moving towards one another below coalescence which cannot be explained using exchange rates only. One possible explanation would be that at least one, probably both, of the observed peaks still consist of at least two chemically not equivalent conformations. If both states possess different energy values a change in temperature leads to a thermodynamically controlled change in distribution. As the sample is given significant time to adjust for temperature changes kinetic effects are assumed to be negligible. As temperature is decreased the Boltzmann distribution is shifted towards the state of lower energy. This is causing the average peak to continuously shift towards the original peak position of the lower energy state. DFT calculations have shown the anti-syn conformation to be energetically favourable by  $2.8 \text{ kcal mol}^{-1}$  for rotation around the  $C_\zeta - N_\eta$  bond. For rotation around the  $C_\zeta - N_\eta$  bond there cannot be a preferred conformation since the guanidino nitrogen conformation is fixed at an 120 degree angle between each N-C bond in the  $sp^2$ -hybridized system. Therefore there cannot be a difference in total energy of the molecule for rotation about the  $C_\zeta - N_\eta$  bond, as either one of the  $N_\epsilon$  groups is always standing cis while the other is in trans conformation in respect to the  $N_\epsilon$  proton. This results in different energies for the side chains itself, but not for the molecule overall.

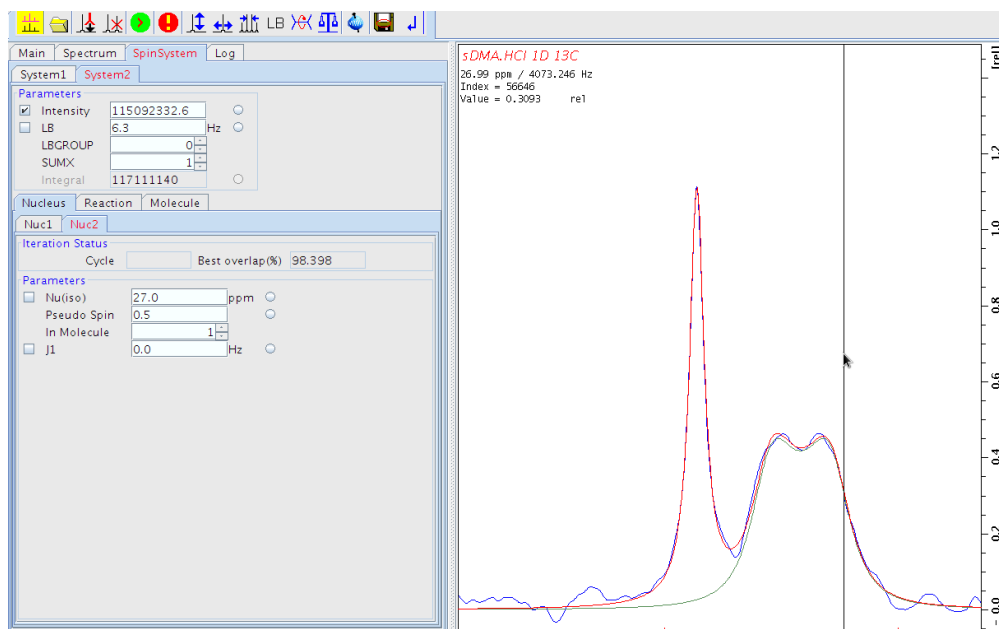
In conclusion, if the first assumption of a chemical shift due to change in Boltzmann distribution is correct, the yet unfrozen rotation has to be around the  $C_\zeta - N_\eta$  bonds. This is consistent with evidence presented earlier supporting the assumption of the reported rotational barrier to correspond to the  $C_\zeta - N_\epsilon$  bond. Another line of evidence supportive of this idea is that as both possible conformational states for  $C_\zeta - N_\eta$  bond rotation are unevenly populated the signals observed in NMR should be of unequal intensity. This is not the case for all reported spectra. As one can see from Scheme 5.8 both signals yield the same integral with  $\ll 1\%$  inaccuracy.



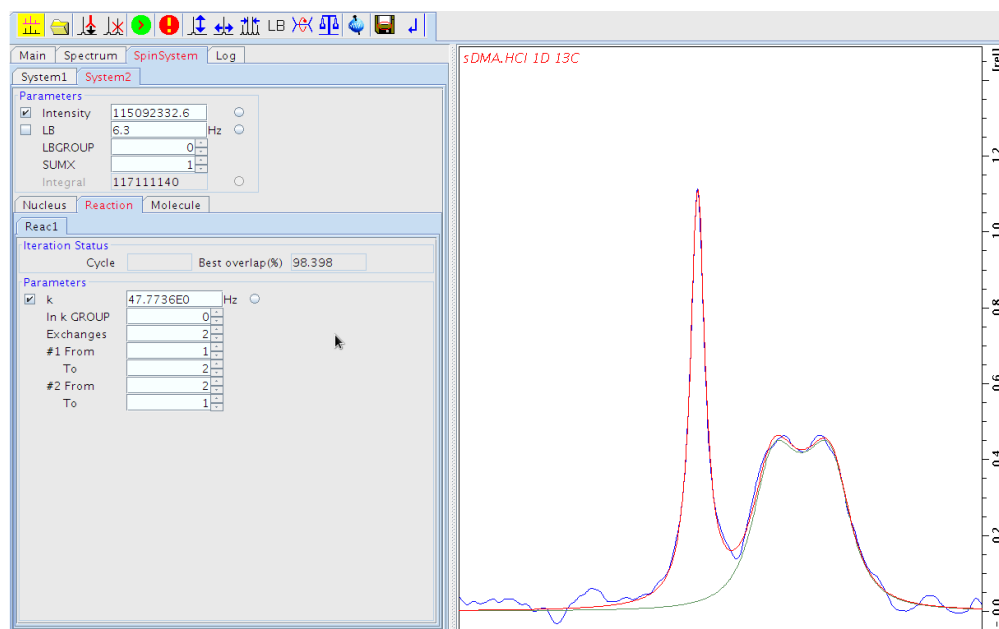
**Scheme 5.8** – Intensity comparison for base line separated peaks

Slight differences are due to inaccuracies while peak picking. The peaks are slightly overlapping and therefore perfect integration is not possible. For the comparison a  $^1H$  spectrum at 220 K was chosen because it firstly gives the best peak separation of all recorded spectra and secondly the Boltzmann distribution would show larger differences in population for lower temperatures. Since there was no second coalescence visible as it should have been when falling below the energy of activation, it is assumed that the energy of activation for  $C_\zeta - N_\eta$  bond rotation is below  $8.9 \text{ kcal mol}^{-1}$ . An estimate of activation energy around the  $C_\zeta - N_\eta$  could be made using computational methods. Since there was only one energy barrier observable in the process further discussions always apply to the  $C_\zeta - N_\epsilon$  bond rotation if not noted otherwise.

For data analysis the spectra are fitted using the TOPSPIN DNMR module 1.1 which gives for example Scheme 5.9 and Scheme 5.10.



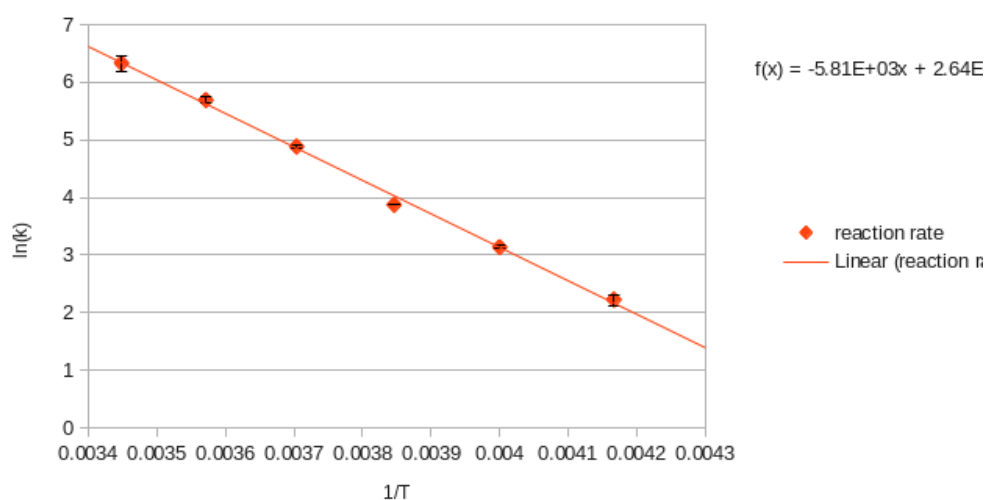
**Scheme 5.9** – Bruker DNMR program with variable line broadening, peak intensity and peak position



**Scheme 5.10** – Bruker DNMR program with variable rate constant and spin system assignment

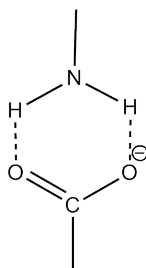
The rate constant can be read out from Scheme 5.10 after there is no significant

change to fitting within 1000 iterations and the parameter optimization is stopped by the system. It is important to notice whether the fit quality is sufficient. A good quality is indicated by a “Best overlap” value greater than 90%. Furthermore it is important to check if fitting line shape and experimental data line shape are in good agreement. Plotting  $\ln(k)$  against  $1/T$  where  $k$  is the rate constant and  $T$  is the measurement temperature gives the Arrhenius plot (Scheme 5.11):



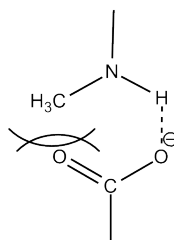
**Scheme 5.11** – Arrhenius diagram for SDMA HCl in methanol- $d_3$

The linear regression equation is given in the spectrum. The slope is  $-5.81 \times 10^3$ . Using 2.4.3 the activation energy is obtained from the linear regression slope. DNMR analysis of the measured data yields an activation energy of  $11.7 \pm 0.4$  kcal mol $^{-1}$  which is a little smaller than for the same rotation in an arginine system. Different to the expectations stated earlier the activation energy does not show an increase but rather a decrease. The decrease is rather small but can be explained when having a look at the isolated arginine system. In earlier papers a 6-membered ring system has been postulated including the guanidine protons and the carboxylate group inside the arginine back bone Scheme 5.12.



**Scheme 5.12** – 6-membered ring created by hydrogen bonding interactions

These hydrogen bonds are broken when methyl groups are introduced into the system. Furthermore there would be repulsion between the added methyl group and a carboxylate side chain Scheme 5.13.



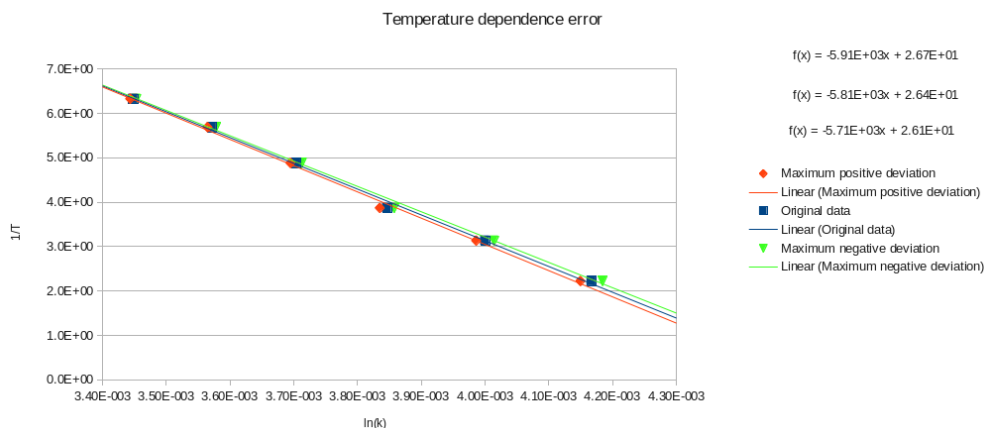
**Scheme 5.13** – The hydrogen bonding interaction is broken apart by arginine methylation

For every rotation including guanidino protons which are all involved in 6-membered rings either hydrogen bonding between guanidino and carboxylate group has to be broken or the whole side chain has to rotate as well. Both of those possibilities significantly increase the amount of energy required to enable partial double bond rotation. Thus the rotation is no longer only limited to a partial double bond character but also dependent on the 6-membered ring's bond strength. The impact of this structural change is the largest on the  $C_\zeta - N_\eta$  bond rotation since its molecular weight is so small amino group rotations usually require quantum mechanical treatment.<sup>[10]</sup> Another possibility is that the used counter ion HCl increases the  $pK_a$  of the solution drastically while reducing the amount of deprotonated carboxylate groups. Inside a natural environment the influence of carboxylate groups should be small as well, since the amount of free, uncondensed carboxylate groups is significantly lower in a protein.

Due to methylation modification the side chain weight is significantly increased. Therefore no quantum mechanical treatment of the obtained data is necessary, as it would be for an  $NH_2$  group, to gain rate constants.

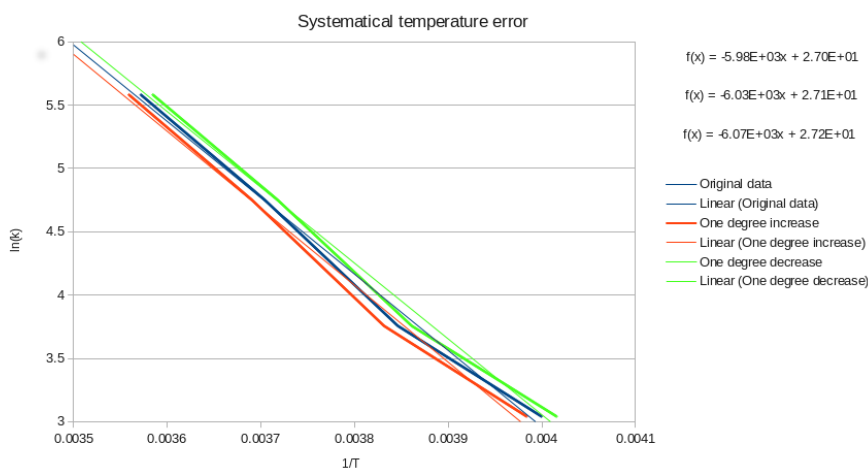
### 5.2.1 Error estimation

To obtain information about the error of this calculation different possible errors have to be identified and their magnitude has to be estimated. Firstly there is an error in temperature calibration. Before each measurement it was waited until the temperature was constant for 25 minutes. The displayed temperature was only off by a maximum of 0.2 K for this temperature range but it is unclear if there is any temperature gradient involved from gas flow to sample core temperature. Another source of temperature error is sample warming due to the measurement itself. Especially decoupling sequences cause an increase in temperature. The error magnitude is not exactly known and a maximum error of 1 K is assumed. If plotting the temperature against rate constant again one gets Scheme 5.14:



**Scheme 5.14** – Uncertainty in activation energy caused by a statistic temperature error

Assuming the greatest possible error is statistic temperature instability of 1 K would yield a measurement uncertainty of  $0.5 \text{ kcal mol}^{-1}$ . This error is quite large but the actual statistical error of the used measurements is around 0.3 K which is composed of temperature inhomogeneities inside the spectrometer as well as fluctuations of at most 0.15 K as reported by the thermometer inside the NMR spectrometer. The error thus becomes  $0.2 \text{ kcal mol}^{-1}$ . The greater error in temperature is systematic. Incorrect temperature calibration as well as sample heating due to decoupling pulses both cause a systematic error. Measurements using chemical shift to temperature calibration curves showed that assuming an error of  $<1 \text{ K}$  is reasonable. Applying this kind of systematic error to the obtained data yields Scheme 5.15:



**Scheme 5.15** – Uncertainty in activation energy caused by a systematic temperature error

The calculated maximum error is very small at  $0.09 \text{ kcal mol}^{-1}$  and therefore negligible.

Secondly there is an error within each fit. Most of the times there is no possible perfect line shape fit. There are often different sets of counteracting parameters like line broadening and rate constant that allow for more than one fit giving plausible results. Furthermore since line broadening and peak position cannot be determined exactly as discussed earlier there is an uncertainty within each fitting parameter. To account for these errors different fits are tried and their rate constants are noted. A range of different activation energy values is obtained when taking other possible rate constants into account and creating several Arrhenius plots. For all these values the activation energy lies within  $11.7 \pm 0.4 \text{ kcal mol}^{-1}$  where the latest is assumed as the total error, since it is significantly larger than error caused by temperature uncertainties.

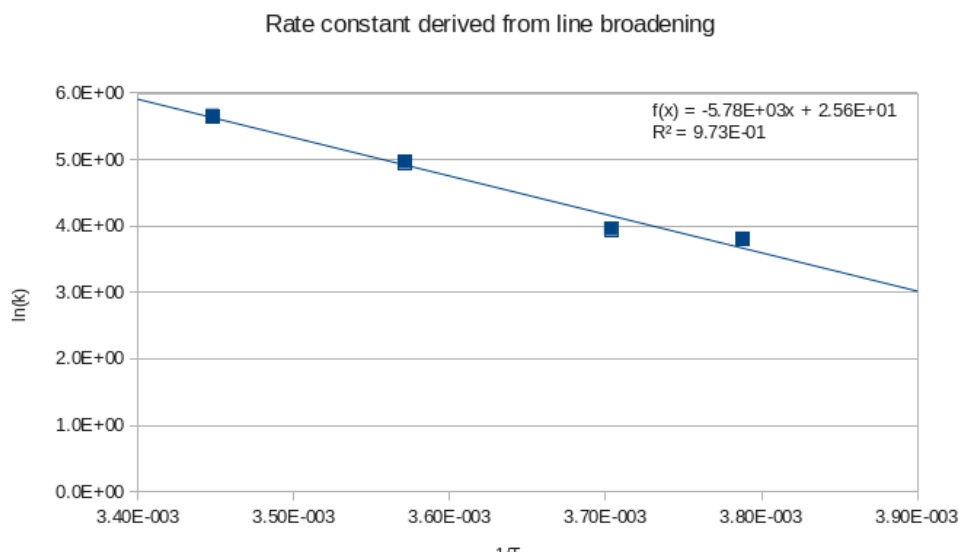
## 5.2.2 Comparison of results with classical line shape analysis

A comparison to the classical DNMR method of simply analysing line broadening is tried. It gives the following rate constant data (Table 5.2).

**Table 5.2** – classical DNMR analysis of sDMA HCl  $CD_3OH$

| <i>Temperature [K]</i> | <i>rate constant [1/s]</i> |
|------------------------|----------------------------|
| 290                    | 285                        |
| 280                    | 143                        |
| 270                    | 52.1                       |
| 264                    | 44.8                       |
| 250                    | 23.9                       |
| 240                    | 9.5                        |

As one can see the rate constant change below and above coalescence is not consistent, making it hard to derive an activation energy value of good quality. This demonstrates one huge advantage of full line shape fitting as possible with various DNMR tools. Simply evaluating the rate constant data above coalescence gives Scheme 5.16:

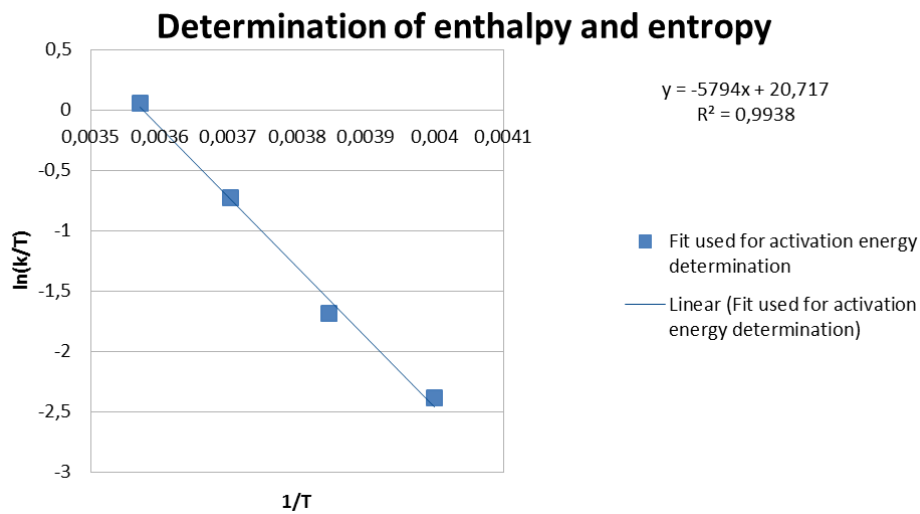


**Scheme 5.16** – Arrhenius plot of rate constant data obtained by classic line broadening analysis

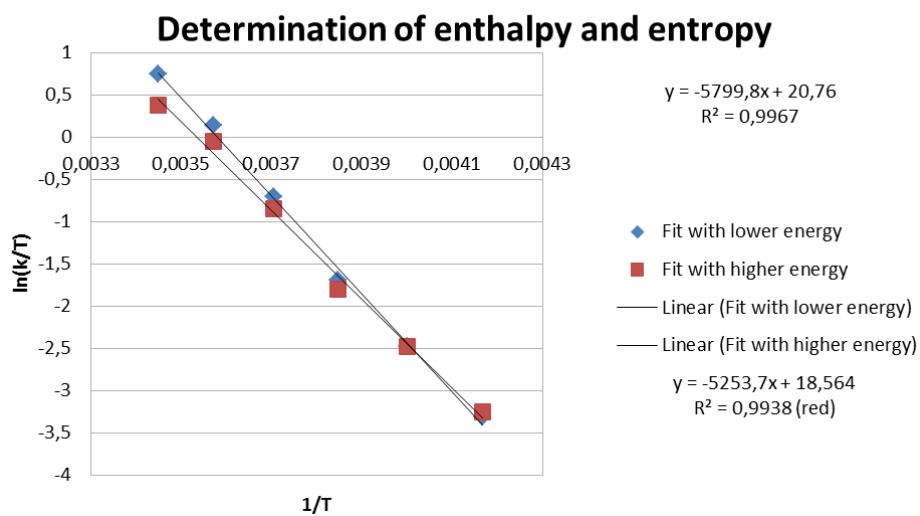
Firstly only four analysable points and secondly a bad linear regression fit, as indicated by an coefficient of determination value below 99%, furthermore show the disadvantages of simple line broadening analysis. The result for activation energy calculations is  $11.5 \text{ kcal mol}^{-1}$ . This is surprisingly close to the value determined before, yet there is no proper error calculation possible. There are also other errors. These include different shim, matching and tuning quality for

each spectrum which result in different line broadening and signal to noise ratios for each measurement. Broader signals have a direct effect on line shape analysis whereas a decreased signal to noise ratio leads to worse line shape fitting. Both have a statistical uncertainty effect on the determined rate constant, but these are negligibly small.

From the collected data the entropy and enthalpy of rotational transition states can be determined. Using 2.4.8 these energies can be determined by linear regression. The required plots for parameter calculation are Scheme 5.17 and Scheme 5.18.



**Scheme 5.17** – Arrhenius plot for determination of transition state entropy and enthalpy

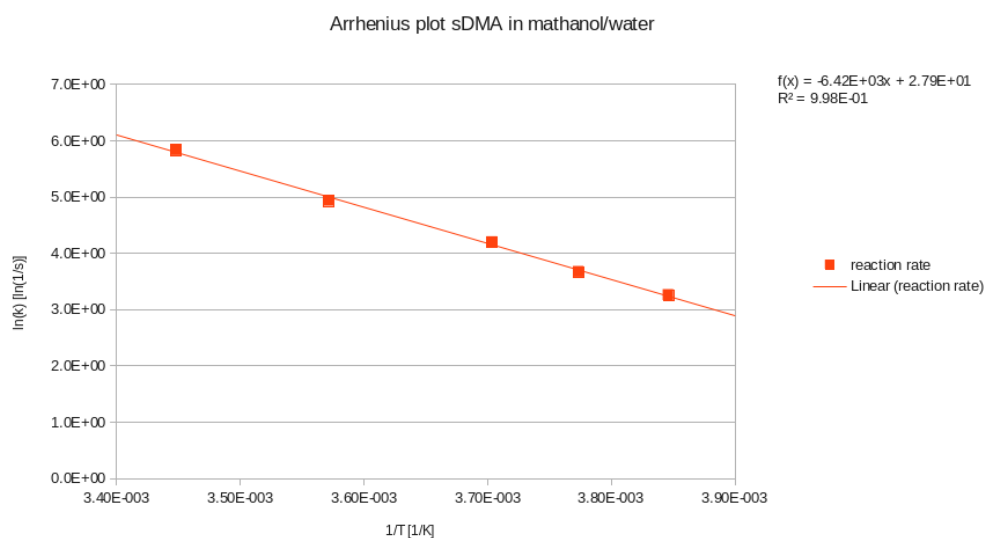


**Scheme 5.18** – Arrhenius plot for determination of error in transition state entropy and enthalpy calculation

These graphs yield an enthalpy of  $11.0 \pm 0.5 \text{ kcal mol}^{-1}$  and an entropy of  $-8 \pm 2 \text{ kcal mol}^{-1}$ . The entropy of activation shows the greatest error. The highest and the lowest obtained entropy and enthalpy define the range in which activation enthalpy and entropy might lie.

### 5.2.3 Investigation of solvent influence on the activation energy

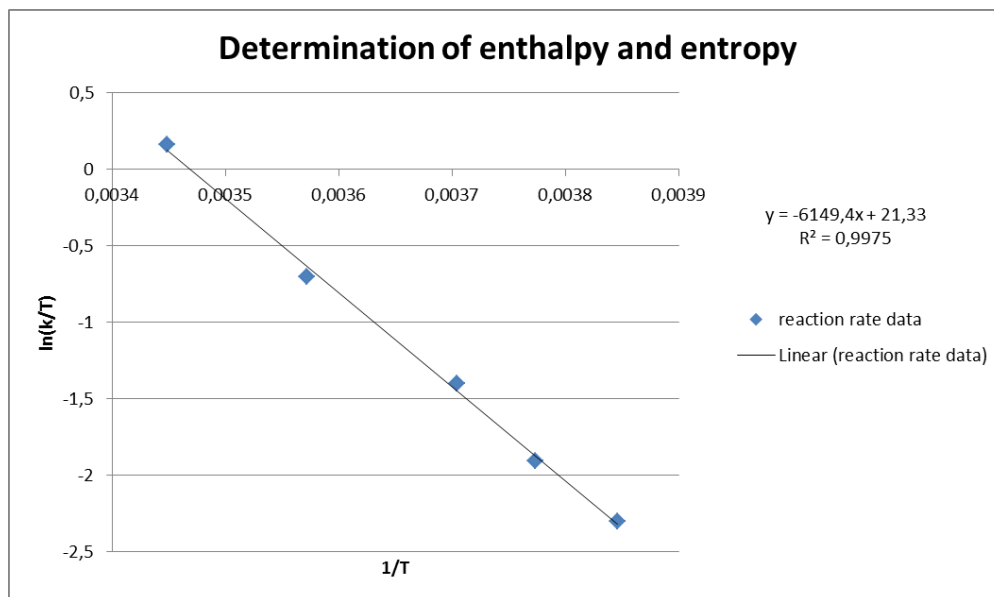
In the following a sample containing 9.1 g of sDMA was solved in 300  $\mu\text{l}$  of distilled water and 99.8%  $\text{CD}_3\text{OH}$  each. Changing the solvent to more natural conditions was done to ensure the assignability of the observed system to biological application. This also allows directly comparing the obtained data to data previously found data for the arginine guanidine system. Applying a DNMR fitting procedure to the corresponding data yields Scheme 5.19 and an activation energy of  $12.8 \pm 0.6 \text{ kcal mol}^{-1}$ .



**Scheme 5.19** – Arrhenius plot sDMA · 2 HCl in mathanol- $\text{d}_3$ /water

This energy of activation is very close to the one discussed earlier. The results still suggest there is a solvent influence on rotational constants of the molecule. This solvent influence can be explained due to different electronic surroundings the two used solvents create. Even though water and methanol are chemically very similar and both possess the possibility to create hydrogen bonding, the water molecules are much smaller and able to create a better hydrogen bonding system. For rotations in a guanidino system hydrogen bonding seems to a largely contributing force. Furthermore there was also no coalescence point visible other than the one discussed above. Great similarity between results gained by analysing data for these two different solutions shows transferability of the obtained data to other polar solvent surroundings. For this solution entropy

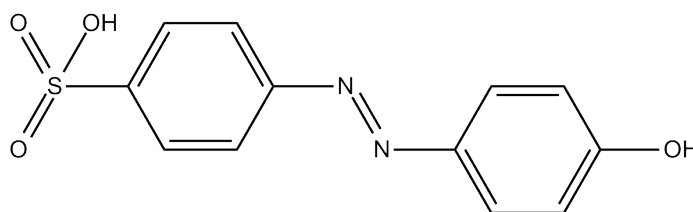
and enthalpy of activation can be determined. Entropy is about  $12.2 \pm 0.5 \text{ kcal mol}^{-1}$  and enthalpy is about  $-5 \pm 2 \text{ kcal mol}^{-1}$ .



**Scheme 5.20** – Enthalpy and Entropy of rotation for sDMA in methanol-d<sub>3</sub>/water

#### 5.2.4 Investigation of counter ion influence on the activation energy

Further solution 3 from Table 5.1 was used to determine the influence of an aromatic counter ion to rotational barriers. If sDMA is recognized by a Tudor domain it is accommodated in an aromatic pocket. Inside the aromatic pocket there is some degree of freedom as the distance to the aromatic side chains accommodating it perpendicularly are 4.0 Å and 3.8 Å respectively as determined by crystal structure analysis<sup>[15]</sup>. The distance to aromatic side chains accommodating sDMA perpendicularly are reported to be even greater with 4.8 Å and 5.8 Å. HABS counter ion is believed to bind to the guanidino group of sDMA. This binding consists of a positive attraction between the partially positively charged guanidino carbon atom and increased electron density of the  $\pi$ -system of HABS. The  $\pi$ -system possesses a negatively charged electron cloud. These oppositely charged groups attract one another.



**Scheme 5.21** – *p*-hydroxyazobenzene – *p'*-sulfonate

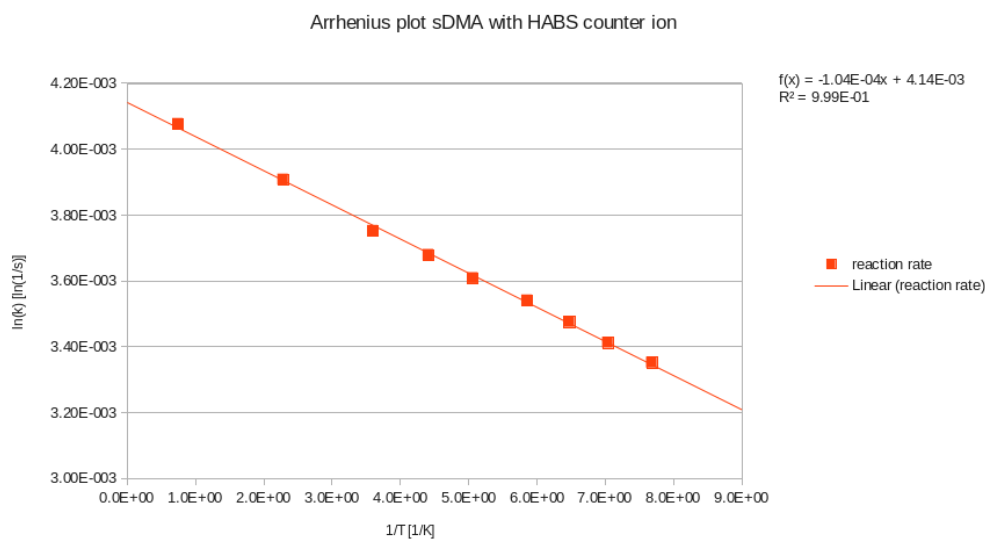
Furthermore there has been a change to the solvent from DMSO to methanol. This exchange of solvents is assumed to have a small influence on the rotational barrier with higher temperatures. But as the temperature gets close to the freezing point of a DMSO/ $H_2O$  solution,  $-50\text{ }^\circ\text{C}$ , the viscosity significantly increases which causes additional line broadening. This additional line broadening can be accounted for using the DNMR tool. Measurements below 230 K could not be done due to possible freezing of the solution. Therefore this solution could not be tested for coalescence at lower temperatures.

One point of coalescence was found at a temperature of 280 K with signal separation below coalescence of ca. 80 Hz. The exact point of coalescence could not be determined, but by comparing with Scheme 2.2 for coalescence and activation energy a rotational barrier of about  $13.5\text{ kcal mol}^{-1}$  is estimated<sup>[1]</sup>. Usually this estimate gives results which are close to about  $1.5\text{ kcal mol}^{-1}$  to the actual activation energy. For these spectra a rotational barrier of  $20.7\text{ kcal mol}^{-1}$  was found using DNMR calculations. This stands in contradiction with the estimate made before.

As the counter ion was different there are two possibilities for this sudden increase in rotational barrier energy. The first possibility is that there actually is a very strong increase because of HABS hindering the guanidino group to rotate. The  $C_\zeta - N_\epsilon$  rotation has to rotate not only a guanidino group but also the HABS counter ions accommodating the guanidino group.

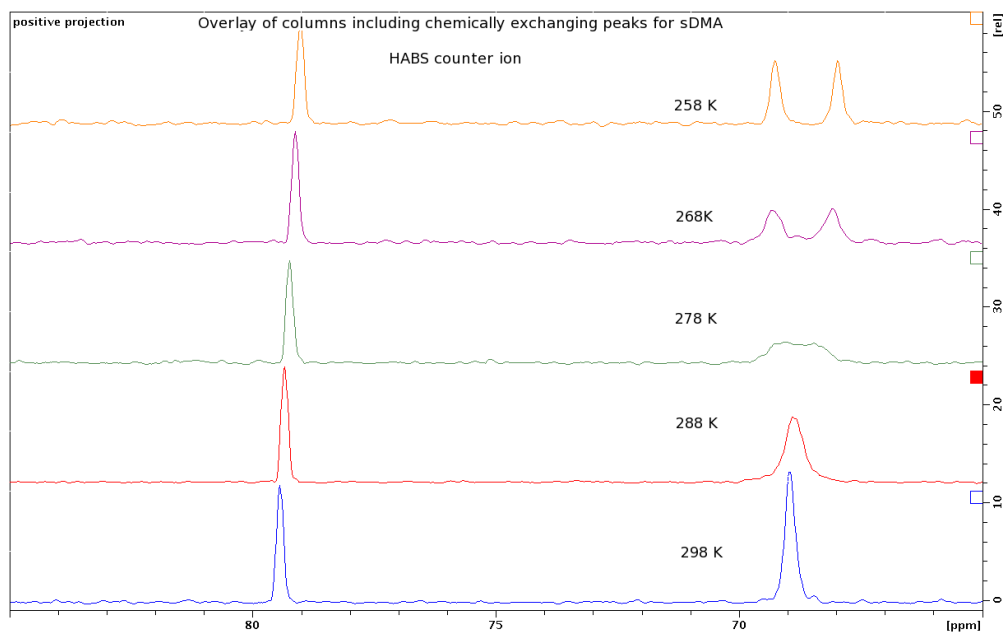
Another possibility is that the increase in rotational energy barrier is a lot smaller, but since the activation energy is taken from a rate constant versus temperature plot effects other than a different Boltzmann energy distribution of particles for different temperatures could influence collected rate constant data. As temperature increases binding of HABS will be decreased due to a lower viscosity and higher overall energy in the solution, thus simultaneously increasing the amount of particles with sufficient energy to overcome a rotational barrier as well as decreasing effective binding of HABS and sDMA. Both processes take place on the experimental temperature scale. There is no proper estimate on how highly binding affinity changes also have an effect on rate constant data, but it will somewhat furthermore increase the rate constant of rotation for higher temperatures causing an overestimation of rotational energy.

Thirdly HABS is far less acidic than HCl. This causes an increase in solution  $pK_a$  subsequently increasing the amount of deprotonated carboxylate groups able to engage in hydrogen bonding. Simply from the estimate made before and the rate constant calculated from Scheme 5.22 one can say that the energy of activation is increased by the addition of an aromatic counter ion.



Scheme 5.22 – Arrhenius diagram sDMA HABS

Compared to both samples containing HCl as a counter ion the maximum peak separation is significantly increased whereas coalescence temperature is only slightly increased.

Scheme 5.23 –  $C_\zeta - N_\eta$  cross peak of sDMA HABS at different temperatures

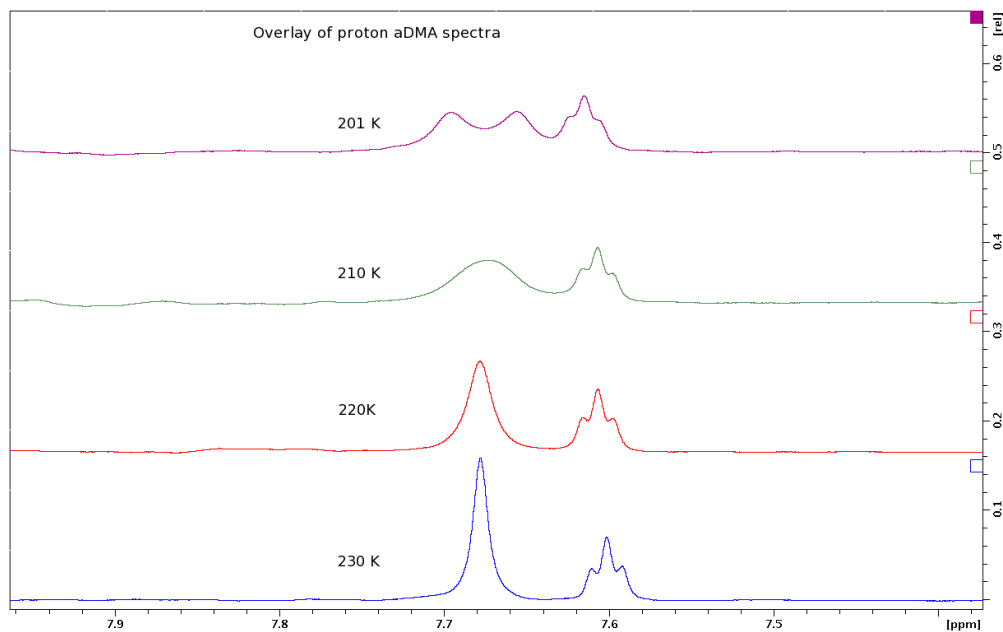
This indicates that conformational change around the  $C_\zeta - N_\eta$  bond is going to be drastically hindered inside the aromatic cage. There is no information about rotation around the  $C_\zeta - N_\eta$  bond obtainable from the given data. But since

hydrogen bonding seems to have a great influence on the rotational barrier this one should be considerably higher when interacting with the negatively charged electron clouds of side chains making up an aromatic pocket. Furthermore a hydrogen bond triangle as suspected by previous papers on sDMA would provide a large force which has to be overcome before rotation can be initiated<sup>[15]</sup>. Hydrogen bonding and bipolar interactions would have to be overcome before rotation can start, which requires a significant amount of energy, for example around  $3 \text{ kcal mol}^{-1}$  per imino to nitrogen bond<sup>[47]</sup>. The possibility that there is no second point of coalescence visible due to an exact overlap of both peaks below coalescence is highly unlikely and therefore ruled out.

As no data set showed more than one coalescence over its entire temperature range the rotational barrier of  $C_\zeta - N_\eta$  bond rotation is probably below  $8.9 \text{ kcal mol}^{-1}$ . With activation energy of this order the inter conformational exchange rate has to be in the thousands of Hz. Thus conformational exchange between anti-anti and anti-syn does not pose any limitation to binding of sDMA in Tudor domains. The limitation of Tudor domain to sDMA modified protein is solely dependent on diffusion forces as well as forces responsible for correct alignment of Tudor domain and recognized protein.

### 5.3 Examination of aDMA data

Data for aDMA is analysed the same way and two temperature series are taken. The one showing greater signal to noise ratio is chosen for evaluation. The point of coalescence is reached at a significantly lower temperature when analysing aDMA data in comparison to sDMA data. This firstly means that the observed rotational barrier is of much lower energy. There is only one point of coalescence visible at a little over 200 K.



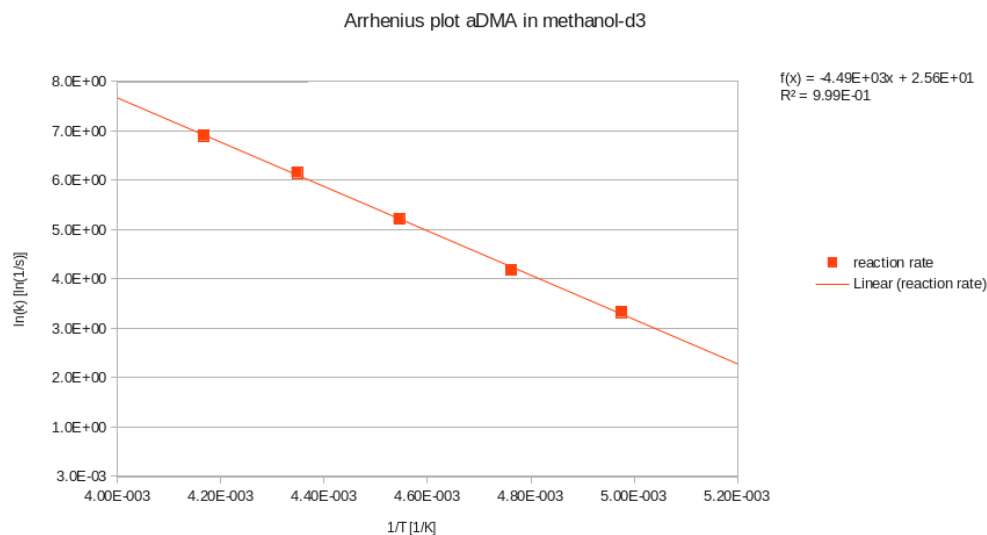
**Scheme 5.24** – Carbon peak of aDMA  $2 \cdot \text{HCl}$  methyl groups at different temperatures

There is also coalescence visible in  $^{13}\text{C}$  spectra about the same temperature range, but the signal-to-noise ratio is a lot worse, making line shape fitting less accurate. After evaluation of the collected  $^1\text{H}$  spectra rate data displayed in Table 5.3 is obtained.

**Table 5.3** – rate constant data for aDMA  $\text{HCl } CD_3OH$

| <i>Temperature</i> [K] | <i>rate constant</i> [1/s] |
|------------------------|----------------------------|
| 240                    | 1000                       |
| 230                    | 473                        |
| 220                    | 185                        |
| 210                    | 65.7                       |
| 201                    | 28.1                       |

An Arrhenius plot was created, Scheme 5.25.

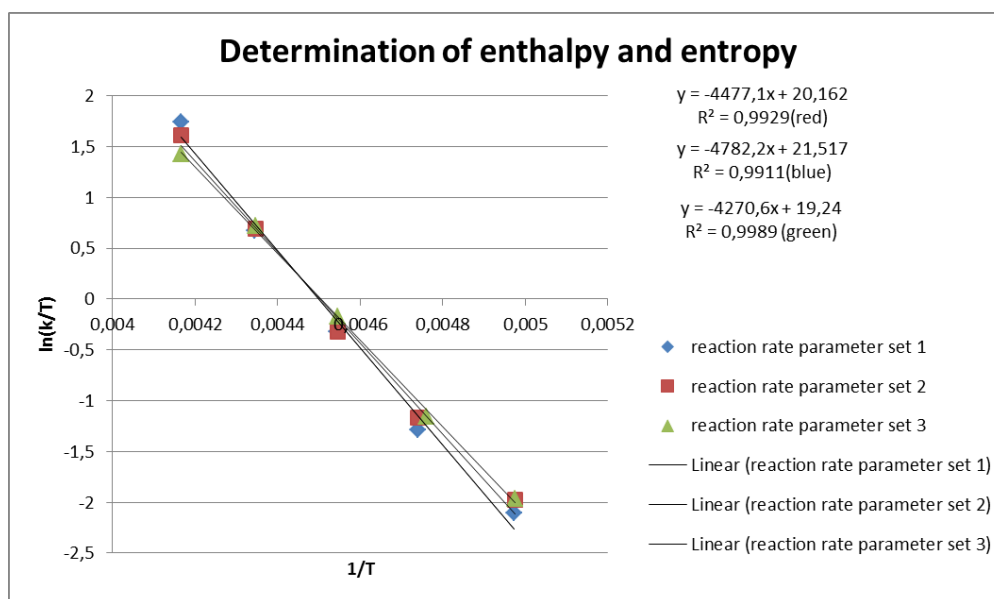


**Scheme 5.25** – Arrhenius diagram for aDMA 2·HCl

The calculated activation energy is  $8.9 \pm 0.9 \text{ kcal mol}^{-1}$ . The error is estimated by applying slightly altered fitting parameters like line broadening change of 0.5 Hz to account for measurement uncertainties. As for previous analysis the error is obtained from an Arrhenius plot using line broadening uncertainty of 0.5 Hz, statistical temperature uncertainty of 0.15 K and a systematic temperature uncertainty of 1 K. It was not possible to determine which rotation is actually observed in these spectra, since any bond rigidity has an influence on all peaks of the guanidino group. Analysing aDMA spectra was very difficult since line broadening at coalescence could not be determined easily. Line broadening was predicted using Scheme 7.1.

Surprisingly there is also no peak coalescence visible at higher temperatures which would have been comparable to arginine side chain rotations. At least the unmodified amino group of the aDMA side chain should show great similarity to the arginine guanidino system. Oddly these similarities do not seem to show. Possible reasons for this are different counter ions and therefore different  $pK_a$  for the tested solution and arginine samples discussed in previous papers<sup>[42,43]</sup>. Higher  $pK_a$  is equivalent with less free carboxylate groups available for hydrogen bonding. Each molecule of aDMA has two HCl molecules bound to it, which are more acidic ( $pK_a = -6$ ) than arginine acid groups ( $pK_a = 2.0$ ), therefore protonating free carboxylate groups. Another possibility is steric hindering of 6 membered hydrogen bond rings, as discussed earlier, by additional methyl groups. This effect is believed to be small and unable to make up for the high difference in activation energy between examined aDMA samples and references for arginine bond rotation.

In this case the observed rotation is most likely to be about the  $C_\zeta - N_\eta$  carrying both methyl groups, since this has to be of higher energy than rotation of the amino group. It is assumed that rotation about  $C_\zeta - N_\epsilon$  bond is not visible in the spectrum, since it would have to possess similar energy to the ones observed before due to the equal weight of the rotating group. The values for activation entropy and enthalpy can be calculated using 2.4.8.



**Scheme 5.26** – Arrhenius plot for determination of transition state entropy and enthalpy for aDMA

Scheme 5.26 yields an enthalpy of  $8.9 \pm 0.5 \text{ kcal mol}^{-1}$  and an entropy of  $-7.0 \pm 2.5 \text{ kcal mol}^{-1}$ .

For the evaluated activation energy conformational exchange is very high at room temperature. Thus inter conformational exchange has no effect on aDMA binding processes.

## 6 Summary

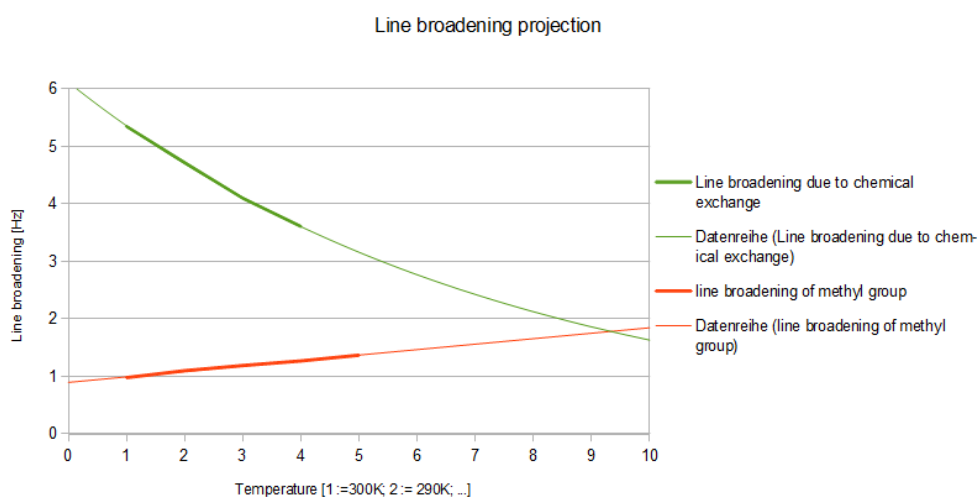
The rotational barrier activation energy results are listed in Table 6.1. In this project different influences on the activation energy of rotation about C-N bonds in the guanidino system have been studied. Throughout the project there was only one point of coalescence visible for every sample set-up. It was concluded that the observed point of coalescence belongs to rotation about the  $C_\zeta - N_\epsilon$  bond, whereas rotation about the  $C_\zeta - N_\eta$  bonds could not be observed. This conclusion could be tested by running computational simulations on the rotation around the  $C_\zeta - N_\epsilon$  and the  $C_\zeta - N_\eta$  bonds and comparing the results for the energies of activation. Another possibility to test this conclusion would be to investigate sDMA and aDMA at lower temperatures to find out if a second point of coalescence will appear. However this would require specialised deep temperature NMR equipment as well as the use of solvents with much lower melting points than methanol. It has been found that a protic and more polar

**Table 6.1** – Summary of activation energy results

| arginine modification | counter ion | solvent                     | activation energy [ $kcal\ mol^{-1}$ ] |
|-----------------------|-------------|-----------------------------|--|
| sDMA                  | HCl         | $CD_3OH$                    | $11.7 \pm 0.4$                         |
| sDMA                  | HCl         | $CD_3OH/H_2O$ (50:50 vol %) | $12.3 \pm 0.6$                         |
| sDMA                  | HABS        | $DMSO/H_2O$ (50:50 vol %)   | ca. 13.3                               |
| aDMA                  | HCl         | $CD_3OH$                    | $8.9 \pm 0.9$                          |

environment increases the activation energy. It has also been found that the addition of an aromatic counter ion (here:HABS) leads to a significant increase in activation energy. For aDMA the observed energy of activation was very low with  $8.9 \pm 0.9$ . The activation energy for  $C_\zeta - N_\eta$  bonds could not be observed and it is assumed that the point of coalescence has to be considerably below the lowest experiment temperature of 200 K. Therefore the activation energy for the  $C_\zeta - N_\eta$  bonds in sDMA has to be significantly below  $8.9\ kcal\ mol^{-1}$  as calculated for aDMA which means that at room temperature conformational exchange will be very fast ( $\gg 1000Hz$ ). Thus rotations around partial double bonds inside the guanidino system do not pose a limitation to binding of proteins with sDMA or aDMA motif to recognition sites (e.g Tudor domains).

## 7 Appendix



**Scheme 7.1** – Prediction of line broadening used for settings in DNMR analysis with aDMA

**Table 7.1** – Pulse length of proton pulse used for acquisition

| temperature [K] | <sup>1</sup> H pulse length<br>sDMA HCl [ $\mu$ s] | <sup>1</sup> H pulse length<br>aDMA HCl [ $\mu$ s] |
|-----------------|--|--|
| 300             | 10.00  | 9.90   |
| 290             | 9.71   | 9.78   |
| 280             | 9.69   | 9.89   |
| 270             | 0.64   | 9.91   |
| 260             | 10.59  | 9.92   |
| 250             | 9.83   | 10.04  |
| 240             | 10.21  | 10.27  |
| 230             | 10.70  | 10.80  |
| 220             | 12.44  | 11.28  |
| 210             | 10.80  | 11.45  |

Table 7.2 – Peak data for aDMA HCl in methanol-d<sub>3</sub>

| Temperature<br>[K] | chemical<br>shift [ppm]                            | CD <sub>3</sub> OH | COOH   | CNH    | NH <sub>2</sub> -<br>backbone | 2xNH(q)<br>guanidino | NH(t)          | H <sub>α</sub> (m) | H <sub>β</sub> (q) | 2xCH <sub>3</sub><br>(dd) | H <sub>β</sub> | H <sub>γ</sub> |
|--------------------|--|--------------------|--------|--------|-------------------------------|----------------------|----------------|--------------------|--------------------|---------------------------|----------------|----------------|
| 298                | <sup>1</sup> H<br><sup>13</sup> C/ <sup>15</sup> N | 4.916              | 170.3  | 156.5  | 8.422                         | 7.40<br>72.44        | 7.318t<br>83.3 | 4.027t<br>52.4     | 3.32<br>41.4       | 3.068<br>37.3             | 2<br>27.4      | 1.805<br>24.5  |
| 280                | <sup>1</sup> H<br><sup>13</sup> C/ <sup>15</sup> N | 5.07               | 170.4  | 156.4  | 8.45<br>76.55                 | 7.47<br>72.41        | 7.388<br>83.09 | 4.039<br>52.36     | 3.33<br>41.3       | 3.062<br>37.3             | 2<br>27.4      | 1.77<br>24.5   |
| 260                | <sup>1</sup> H<br><sup>13</sup> C/ <sup>15</sup> N | 5.24               | 170.5  | 156.3  | 8.48<br>76.12                 | 7.54<br>72.37        | 7.45<br>82.89  | 4.046<br>52.3      | 3.328<br>41.2      | 3.059<br>37.3             | 2.02<br>27.4   | 1.76<br>24.4   |
| 240                | <sup>1</sup> H<br><sup>13</sup> C/ <sup>15</sup> N | 5.39               | 170.55 | 156.14 | 8.51                          | 7.61                 | 7.52t          | 4.06               | 3.325              | 3.052                     | 1.97           | 1.76           |
| 220                | <sup>1</sup> H<br><sup>13</sup> C/ <sup>15</sup> N | 5.52               | 170.6  | 156    | 8.52                          | 7.66                 | 7.59           | 4.065              | 3.317              | 3.04                      | 1.96           | 1.71           |
|                    |  |                    |        |        |                               |                      |                | 52.1               | 41.1               | 37.3                      | 27.3           | 24.4           |

**Table 7.3** – Peak data for sDMA HCl in methanol-d<sub>3</sub>

| Temperature [K] | chemical shift [ppm]             | CD <sub>3</sub> OH | COOH   | CNH    | NH <sub>2</sub> -backbone | 2xNH(q)guanidino | NH(t) | H <sub>α</sub> (m) | H <sub>δ</sub> (q) | Methyls (dd)               | H <sub>β</sub> | H <sub>γ</sub> |
|-----------------|----------------------------------|--------------------|--------|--------|---------------------------|------------------|-------|--------------------|--------------------|----------------------------|----------------|----------------|
| 310             | <sup>1</sup> H                   | 4.8                |        |        | 8.4                       | 7.33             | 7.28  | 4.025              | 3.31               | 2.89/2.88                  | 2.01           | 1.81           |
|                 | <sup>13</sup> C/ <sup>15</sup> N |                    | 170.3  | 156.1  | 69                        | 80.15            | 80.1  | 52.5               | 40.5               | 27.174/<br>26.981          | 27.4           | 24.5           |
| 300             | <sup>1</sup> H                   | 4.9                |        |        | 8.42                      | 7.37             | 7.32  | 4.03               | 3.31               | 2.89/2.88                  | 2              | 1.81           |
|                 | <sup>13</sup> C/ <sup>15</sup> N |                    | 170.3  | 156.1  | 69                        | 80.07            | 80.07 | 52.4               | 40.5               | 27.156                     | 27.4           | 24.4           |
| 290             | <sup>1</sup> H                   | 4.99               |        |        | 8.43                      | 7.40             | 7.36  | 4.03               | 3.304              | 2.884/2.876                | 2              | 1.79           |
|                 | <sup>13</sup> C/ <sup>15</sup> N |                    | 170.4  | 156    | 80                        | 68.9             | 80    | 52.4               | 40.4               | 27.14                      | 27.4           | 24.4           |
| 280             | <sup>1</sup> H                   | 5.07               |        |        | 8.45                      | 7.44             | 7.41  | 4.04               | 3.33               | 2.87                       | 2              | 1.78           |
|                 | <sup>13</sup> C/ <sup>15</sup> N |                    | 170.4  | 155.9  | 76.5                      | 68.8             | 79.9  | 52.4               | 40.4               | 27.1                       | 27.4           | 24.4           |
| 270             | <sup>1</sup> H                   | 5.16               |        |        | 8.46                      | 7.48q            | 7.45t | 4.04q              | 3.30q              | 2.87                       | 1.99           | 1.776          |
|                 | <sup>13</sup> C/ <sup>15</sup> N |                    | 170.4  | 155.9  | 80                        | 68.5/69.1        | 79.85 | 52.3               | 40.4               | 27.1                       | 27.4           | 24.4           |
| 260             | <sup>1</sup> H                   | 5.237              |        |        | 8.48                      | 7.52             | 7.5   | 4.05               | 3.30q              | 2.87                       | 1.97           | 1.77           |
|                 | <sup>13</sup> C/ <sup>15</sup> N |                    | 170.5  | 155.8  | 76.1                      | 68.2/69.2        | 79.8  | 52.3               | 40.3               | 27.1                       | 27.4           | 24.4           |
| 250             | <sup>1</sup> H                   | 5.316              |        |        | 8.49                      | 7.54             | 7.52  | 4.06               | 3.29q              | 2.88,2.87<br>2.85,2.84     | 1.98           | 1.76           |
|                 | <sup>13</sup> C/ <sup>15</sup> N |                    | 170.5  | 155.7  | 76                        | 69.2/68.1        | 79.7  | 52.24              | 40.3               | 27.2/27.0                  | 27.4           | 24.3           |
| 240             | <sup>1</sup> H                   | 5.39               |        |        | 8.5                       | 7.58             | 7.57  | 4.07               | 3.29q              | 2.85                       | 1.98           | 1.75           |
|                 | <sup>13</sup> C/ <sup>15</sup> N |                    | 170.5  | 155.6  | 75.8                      | 69.1/68.0        | 79.6  | 52.2               | 40.3               | 27.2/27.0                  | 27.3           | 24.3           |
| 230             | <sup>1</sup> H                   | 5.46               |        |        | 8.51                      | 7.62             | 7.62  | 4.065q             | 3.28q              | 2.87,2.86<br>2.84,2.83     | 1.97           | 1.73           |
|                 | <sup>13</sup> C/ <sup>15</sup> N |                    | 170.6  | 155.6  | 79.6                      | 69.1/68.0        | 79.6  | 52.17              | 40.2               | 27.174/<br>26.981          | 27.3           | 24.3           |
| 220             | <sup>1</sup> H                   | 5.52               |        |        | 8.52                      | 7.64             | 7.65  | 4.07               | 3.28q              | 2.866,2.858<br>2.835,2.872 | 1.97           | 1.73           |
|                 | <sup>13</sup> C/ <sup>15</sup> N |                    | 170.6  | 155.5  | 75.5                      | 69.0/67.8        | 79.5  | 52.1               | 40.2               | 27.165/<br>26.977          | 27.3           | 24.3           |
| 210             | <sup>1</sup> H                   | 5.6                |        |        | 8.5                       | 7.67/7.67        | 7.68  | 4.08               | 3.28q              | 2.86,2.85<br>2.83,2.82     | 1.96           | 1.71           |
|                 | <sup>13</sup> C/ <sup>15</sup> N |                    | 170.65 | 155.45 | 75.2                      | 69.0/67.7        | 79.5  | 52.1               | 40.2               | 27.158/26.97               | 27.3           | 24.3           |

## List of Schemes

|      |  |    |
|------|--|----|
| 1.1  | Examined bond rotations of sDMA and aDMA . . . . .   | 3  |
| 1.2  | Resonance structures of aDMA . . . . .   | 3  |
| 1.3  | Resonance structures of sDMA . . . . .   | 4  |
| 2.1  | 270 MHz proton NMR of L-arginine HCl in 7 mM sodium acetate and 3.5 mM Na <sub>2</sub> EDTA and 30% CD <sub>3</sub> OH at pH 5.3; arginine concentration is 70 mM; image taken from <sup>[9]</sup> . . . . . | 7  |
| 2.2  | Actiation energy as a funtion of peak separation and temperature <sup>[1]</sup>  | 11 |
| 2.3  | Example for DNMR measurements for rotation about a partial double bond <sup>[1]</sup> . . . . .  | 11 |
| 3.1  | Modification of arginine to sDMA and aDMA by PRMTs . . . . .   | 15 |
| 3.2  | Crystal structure of aromatic pocket taken from <sup>[15]</sup> . . . . .  | 16 |
| 5.1  | <sup>13</sup> C spectrum of sDMA methanol-d <sub>3</sub> at 280K . . . . .   | 21 |
| 5.2  | <sup>1</sup> H spectrum of sDMA methanol-d <sub>3</sub> at 280K . . . . .  | 22 |
| 5.3  | <sup>1</sup> H spectrum of sDMA methanol-d <sub>3</sub> at 280K showing close up of methyl peaks . . . . .   | 23 |
| 5.4  | <sup>1</sup> H- <sup>13</sup> N spectrum of sDMA methanol-d <sub>3</sub> at 310K . . . . .   | 24 |
| 5.5  | <sup>1</sup> H- <sup>15</sup> C spectrum of sDMA methanol-d <sub>3</sub> at 280K . . . . .   | 24 |
| 5.6  | Different possible conformations for aDMA(left) and sDMA(right) by courtesy of M. Sattler . . . . .  | 25 |
| 5.7  | Below coalescence the chemical shift between both methyl peaks is changing . . . . .   | 26 |
| 5.8  | Intensity comparison for base line separated peaks . . . . .   | 28 |
| 5.9  | Bruker DNMR program with variable line broadening, peak intensity and peak position . . . . .  | 29 |
| 5.10 | Bruker DNMR program with variable rate constant and spin system assignment . . . . .   | 29 |
| 5.11 | Arrhenius diagram for SDMA HCl in methanol-d <sub>3</sub> . . . . .  | 30 |
| 5.12 | 6-membered ring created by hydrogen bonding interactions . . . . .   | 30 |
| 5.13 | The hydrogen bonding interaction is broken apart by arginine methylation . . . . .   | 31 |
| 5.14 | Uncertainty in activation energy caused by a statistic temperature error . . . . .   | 32 |
| 5.15 | Uncertainty in activation energy caused by a systematic temperature error . . . . .  | 32 |
| 5.16 | Arrhenius plot of rate constant data obtained by classic line broadening analysis . . . . .  | 34 |

---

|      |  |    |
|------|--|----|
| 5.17 | Arrhenius plot for determination of transition state entropy and enthalpy . . . . .                      | 35 |
| 5.18 | Arrhenius plot for determination of error in transition state entropy and enthalpy calculation . . . . . | 35 |
| 5.19 | Arrhenius plot sDMA · 2 HCl in methanol-d <sub>3</sub> /water . . . . .                                  | 36 |
| 5.20 | Enthalpy and Entropy of rotation for sDMA in methanol-d <sub>3</sub> /water                              | 37 |
| 5.21 | <i>P</i> – <i>hydroxyazobenzene</i> – <i>p'</i> – <i>sulfonate</i> . . . . .                             | 37 |
| 5.22 | Arrhenius diagram sDMA HABS . . . . .  | 39 |
| 5.23 | $C_\zeta - N_\eta$ cross peak of sDMA HABS at different temperatures . .                                 | 39 |
| 5.24 | Carbon peak of aDMA 2·HCl methyl groups at different temperatures . . . . .                              | 41 |
| 5.25 | Arrhenius diagram for aDMA 2·HCl . . . . .   | 42 |
| 5.26 | Arrhenius plot for determination of transition state entropy and enthalpy for aDMA . . . . .             | 43 |
| 7.1  | Prediction of line broadening used for settings in DNMR analysis with aDMA . . . . .                     | 45 |

# List of Tables

|     |  |    |
|-----|--|----|
| 2.1 | Gyromagnetic ratios for nuclei observed during experiments . . . | 5  |
| 5.1 | sample setup . . . . .   | 21 |
| 5.2 | classical DNMR analysis of sDMA HCl $CD_3OH$ . . . . .           | 34 |
| 5.3 | rate constant data for aDMA HCl $CD_3OH$ . . . . .               | 41 |
| 6.1 | Summary of activation energy results . . . . .                   | 44 |
| 7.1 | Pulse length of proton pulse used for aquisition . . . . .       | 45 |
| 7.2 | Peak data for aDMA HCl in methanol- $d_3$ . . . . .              | 46 |
| 7.3 | Peak data for sDMA HCl in methanol- $d_3$ . . . . .              | 47 |

---

## List of abbreviations and acronyms

|                  |   |
|------------------|---|
| <b>1D, 2D</b>    | one-, two-dimensional   |
| <b>DFT</b>       | density functional theory   |
| <b>DMC</b>       | density matrix calculations   |
| <b>sDMA</b>      | symmetrically dimethylated arginine   |
| <b>aDMA</b>      | anti symmetrically methylated arginine  |
| <b>PTM</b>       | post-translational modification   |
| <b>PRMT</b>      | protein arginine methylation transferase  |
| <b>SMN</b>       | survival motor neuron protein   |
| <b>SPF30</b>     | splicing factor 30  |
| <b>mRNA</b>      | messenger ribonucleic acid  |
| <b>CA150</b>     | cancer antigen 150  |
| <b>PIWI</b>      | P-element induced wimpy testis proteins   |
| <b>piRNA</b>     | PIWI interacting RNA  |
| <b>HeLa</b>      | cell type in an immortal human cell line  |
| <b>SND1</b>      | staphylococcal nuclease domain-containing protein 1                             |
| <b>HABS</b>      | <i>p</i> – hydroxyazobenzene – <i>p'</i> – sulfonate                            |
| <b>WATERGATE</b> | water suppression by Gradient-Tailored Excitation                               |
| <b>Sm</b>        | protein rings that function as scaffolds or chaperones for RNA oligonucleotides |
| <b>NMR</b>       | nuclear magnetic resonance  |
| <b>DNMR</b>      | dynamic nuclear magnetic resonance  |
| <b>HSQC</b>      | heteronuclear Single Quantum Coherence  |
| <b>HMBC</b>      | heteronuclear Multiple Bond Correlation   |
| <b>s</b>         | singlet   |

## List of Tables

---

**d** doublet

**dd** doublet of doublets

**t** triplet

**q** quintet

**quin** quintet

**sept** septet

**m** multiplet

# Bibliography

- [1] Reich, H.; *Script to lecture "Structure Determination Using NMR"*; 2011.  
<http://www.chem.wisc.edu/areas/reich/nmr/08-tech-03-dnmr.html>.
- [2] Prof. Dr. Ulrich Heiz; *Script to lecture "Spektroskopie und Photochemie"*; 2013.
- [3] Günther, H. *Angewandte Chemie* **1976**, *88*, 455–455.
- [4] Frahm, J. *Berichte der Bunsengesellschaft für Physikalische Chemie* **1982**, *86*, 873–873.
- [5] R. Ernst, G. Bodenhausen, A. W. *Principles of Nuclear Magnetic Resonance in One and Two Dimensions*; Clarendon Press: Oxford, 1987.
- [6] J. I. Kaplan, G. F. *Angewandte Chemie* **2006**, *94*, 653–654.
- [7] Crabtree, B. *J. Am. Chem. Soc.* **1967**, *89*, 5384.
- [8] Shiotani, A.; Klein, H. F.; Schmidbauer, H. *J. Am. Chem. Soc.* **1971**, *93*, 1555.
- [9] Klevan, L.; Crothers, D. M. *Biopolymers* **1979**, *18*, 1029–1044.
- [10] Eloranta, D. J.; *Dynamic NMR spectroscopy CalState Univ Northridge Lab. Course*; 2010.
- [11] I.O. Sutherland *Academic Press* **1971**, *4*.
- [12] R.S. Dumont, S. Jain, A. B. *J. Chem. Phys.* **1997**, *106*, 5928–5936.
- [13] Rohonczy, J.; Ph.D. thesis; Eötvös Loránd University, Hungary; 1997.
- [14] Chen, C.; Nott, T. J.; Jin, J.; Pawson, T. *Nature Reviews. Molecular Cell Biology* **2011**, *12*, 629–42.
- [15] Tripsianes, K.; Madl, T.; Machyna, M.; Fessas, D.; Englbrecht, C.; Fischer, U.; Neugebauer, K. M.; Sattler, M. *Nature Structural & Molecular Biology* **2011**, *18*, 1414–20.
- [16] Bedford, M. T.; Clarke, S. G. *Molecular Cell* **2009**, *33*, 1–13.

- [17] Siomi, M. C.; Mannen, T.; Siomi, H. *Genes & Development* **2010**, *24*, 636–46.
- [18] Bühler, D.; Raker, V.; Lührmann, R.; Fischer, U. *Human Molecular Genetics* **1999**, *8*, 2351–7.
- [19] Pellizzoni, L.; Kataoka, N.; Charroux, B.; Dreyfuss, G. *Cell* **1998**, *95*, 615–24.
- [20] Pellizzoni, L., Yong, J. & Dreyfuss, G. *Science* **2002**, 1775–1779.
- [21] Singh, N. N.; Shishimorova, M.; Cao, L. C.; Gangwani, L.; Singh, R. N. *RNA Biology*, *6*, 341–50.
- [22] Meister, G.; Hannus, S.; Plöttner, O.; Baars, T.; Hartmann, E.; Fakan, S.; Laggerbauer, B.; Fischer, U. *The EMBO Journal* **2001**, *20*, 2304–14.
- [23] Rappsilber, J.; Ajuh, P.; Lamond, a. I.; Mann, M. *The Journal of Biological Chemistry* **2001**, *276*, 31142–50.
- [24] Cheng, D.; Côté, J.; Shaaban, S.; Bedford, M. T. *Molecular Cell* **2007**, *25*, 71–83.
- [25] Vallance, P.; Leone, A.; Calver, A.; Collier, J.; Moncada, S. *Lancet* **1992**, *339*, 572–5.
- [26] Böger, R. H.; Bode-Böger, S. M.; Thiele, W.; Junker, W.; Alexander, K.; Frölich, J. C. *Circulation* **1997**, *95*, 2068–74.
- [27] Boger, R. H.; Bode-Boger, S. M.; Szuba, a.; Tsao, P. S.; Chan, J. R.; Tangphao, O.; Blaschke, T. F.; Cooke, J. P. *Circulation* **1998**, *98*, 1842–1847.
- [28] Kielstein JT, Bode-Böger SM, Frölich JC, Haller H, B. R. *Kidney Int* **2001**, *59*, 9–13.
- [29] Zoccali, C.; Benedetto, F. A.; Maas, R.; Mallamaci, F.; Tripepi, G.; Malatino, L. S.; Böger, R. *Journal of the American Society of Nephrology : JASN* **2002**, *13*, 490–6.
- [30] Chang, B.; Chen, Y.; Zhao, Y.; Bruick, R. K. *Science (New York, N.Y.)* **2007**, *318*, 444–7.
- [31] Webby, C. J. *Science (New York, N.Y.)* **2009**, *325*, 90–3.
- [32] Brahms, H.; Meheus, L.; de Brabandere, V.; Fischer, U.; Lührmann, R. *RNA (New York, N.Y.)* **2001**, *7*, 1531–42.

- 
- [33] Côté, J.; Richard, S. *The Journal of Biological Chemistry* **2005**, *280*, 28476–83.
- [34] Reuter, M.; Chuma, S.; Tanaka, T.; Franz, T.; Stark, A.; Pillai, R. S. *Nature Structural & Molecular Biology* **2009**, *16*, 639–46.
- [35] Vagin, V. V.; Wohlschlegel, J.; Qu, J.; Jonsson, Z.; Huang, X.; Chuma, S.; Girard, A.; Sachidanandam, R.; Hannon, G. J.; Aravin, A. A. *Genes & Development* **2009**, *23*, 1749–62.
- [36] Mecozzi, S.; West, a. P.; Dougherty, D. a. *Proc. Nat. Acad. Sci. USA* **1996**, *93*, 10566–71.
- [37] Gallivan, J. P.; Dougherty, D. A. *Proc. Nat. Acad. Sci. USA* **1999**, *96*, 9459–9464.
- [38] Dr. Janos Rohonczy, Dr. Teodor Parella; *BRUKER NMR Guide & Encyclopedia*; 2009. <http://www.nmr.unsw.edu.au/guide/tutorials/solvent/w5.html>.
- [39] Dr. Janos Rohonczy, Dr. Teodor Parella; *BRUKER NMR Guide & Encyclopedia*; 2009. <http://www.nmr.unsw.edu.au/guide/tutorials/13cnmr/c13.html>.
- [40] Dr. Janos Rohonczy, Dr. Teodor Parella; *BRUKER NMR Guide & Encyclopedia*; 2009. <http://www.nmr.unsw.edu.au/guide/tutorials/2Dhet/invietgs.html>.
- [41] Dr. Janos Rohonczy, Dr. Teodor Parella; *BRUKER NMR Guide & Encyclopedia*; 2009. <http://www.nmr.unsw.edu.au/guide/tutorials/2Dhet/invietgs.html>.
- [42] Xiao, Y.; Braiman, M. *The Journal of Physical Chemistry. B* **2005**, *109*, 16953–8.
- [43] Sapse, M. *J. Org. Chem.* **1981**, *126*, 2330–2333.
- [44] Kanamori, K.; Roberts, J. D. *J. Am. Chem. Soc.* **1983**, *105*, 4698–4701.
- [45] Henry, G. D.; Sykes, B. D. *Journal of Biomolecular NMR* **1995**, *6*, 59–66.
- [46] Henry, G. D.; Sykes, B. D. *Journal of Biomolecular NMR* **1995**, *6*, 59–66.
- [47] Legon, A. C.; Millen, D. J. *Chemical Society Reviews* **1987**, *16*, 467.

## Ehrenwörtliche Erklärung

Hiermit versichere ich ehrenwörtlich durch meine Unterschrift, dass ich die vorliegende Bachelor's Thesis selbständig und ohne Benutzung anderer als der angegebenen Hilfsmittel und Quellen angefertigt habe. Die aus fremden Quellen direkt oder indirekt übernommenen Gedanken sind als solche kenntlich gemacht. Diese Bachelor's Thesis hat in gleicher oder ähnlicher Form keiner anderen Prüfungsbehörde vorgelegen.

---

Ort, Datum

---

Unterschrift